UNIVERSITY OF OTAGO

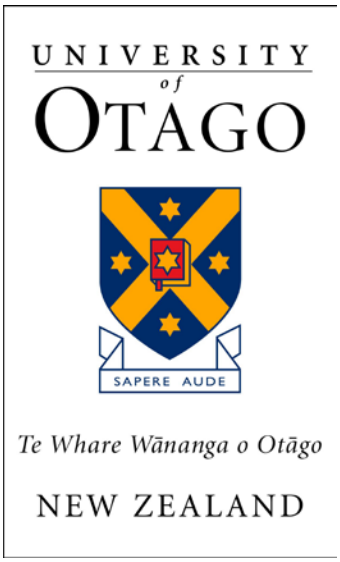

MUTATIONS IN THE WNT MEDIATOR, *DVL1*, CAUSE AN OSTEOSCLEROTIC FORM OF ROBINOW SYNDROME

Kieran James Bunn

A THESIS SUBMITTED FOR THE DEGREE OF BACHELOR OF MEDICAL SCIENCE WITH HONOURS

2015

ABSTRACT

This project aimed to clinically and biochemically characterise a novel phenotype which we have named Robinow Syndrome – Osteosclerotic type (RS-OS). Robinow Syndrome (RS) is a rare form of mesomelic dwarfism defined by a distinctive facial gestalt known as "fetal facies" – a combination of features including hypertelorism and midface hypoplasia. RS can be caused by loss-of-function mutations in genes encoding components of planar cell polarity WNT signalling. Osteosclerosis is associated with gain-of-function mutations in mediators of a different aspect of WNT signalling, the canonical WNT pathway.

This thesis details three sporadic cases of RS-OS. Before this project began a combination of next generation and Sanger sequencing identified that two of these individuals had similar heterozygous *de novo* mutations in gene for the pan-WNT component DVL1, which has not previously been associated with RS. A third case was identified during this project and Sanger sequencing revealed another, similar, *de novo* mutation in *DVL1*. All three *DVL1* mutations fall within the 14th exon and cause a -1 frameshift which predicts a DVL1 product with the wild type C-terminal sequence replaced by a novel amino acid sequence, which is shared across all three affected individuals. We hypothesised that these *DVL1* mutations cause osteosclerosis through a gain-of-function leading to an increase in canonical WNT signalling.

Transcript from cell lysates of cultured dermal fibroblasts taken from an affected individual were analysed by Sanger sequencing and restriction enzyme digest revealed that the mutation-bearing mRNA was endogenously expressed. Transient transfection of mouse C2C12 cells with EGFP-tagged DVL1 constructs showed similar protein levels between mutant and wild type *DVL1* with fluorescent Western blotting. Taken together these experiments showed that the mutant allele is endogenously transcribed as a persistent mRNA, and that the majority of the protein product of that transcript is stable.

Canonical WNT signalling was studied with a transient transfection-based TOPFlash assay. These revealed that, paradoxical to the osteosclerotic phenotype, the mutant DVL1 was significantly less active in the canonical WNT pathway than wild type DVL1. However the co-expression of the mutant DVL1 alongside the wild type DVL1 lead to a significant (~3-fold, $P < 0.01$) increase in canonical WNT activity over the same amount of wild type *DVL1* expressed alone. This co-expression may explain the clinical osteosclerosis: the affected individuals are heterozygous for the *DVL1* mutations thus are likely to co-express mutant and wild type *DVL1*.

This work establishes that novel mutations in *DVL1*, a gene previously not associated with RS, causes an osteosclerotic form of RS. These mutations are likely to lead to osteosclerosis through a gain-of-function mechanism, with an increase in canonical WNT signalling. However this gain-of-function, *in vitro*, depends upon the presence of wild type *DVL1* alongside the mutant *DVL1*. This wild type-dependent gain-of-function is, to our knowledge, unique amongst Mendelian disorders.

ACKNOWLEDGEMENTS

Firstly and foremost I would like to thank my supervisor, Stephen Robertson. Throughout the year his kind and careful guidance has been invaluable, both in shaping this project, and in considering my future.

Phillip Daniel also well deserves my gratitude. He supervised the laboratory aspects of this project, patiently and kindly guiding my through techniques and helpfully advising throughout the numerous problems I encountered. I have thoroughly enjoyed working with him, and his guidance has allowed this year to be a success culminating with our joint first-authorship on a manuscript, which is currently in review.

I would also like to extend my thanks to the other members of the Robertson Laboratory who have made me feel welcome and assisted me. In particular I have worked directly with Tim Morgan, Sophia Cameron-Christie, Christine Neyt, Adam O'Neill, Zandra Jenkins, and Emma Wade.

A number of people not named above have also collaborated with me over two publications and for their input and assistance I would like to thank: Susan Craw, Azza Al-Ani, Angeline Lai, Mauro Farella, Heleen Rösken, Han Brunner, Henricus Kunst, and David Markie. Both Alan Carne and Julia Horsfield also aided in collaborations, which shaped the thinking that went into this work. I am forever grateful to Warren Tate, who supervised me through a previous Summer Studentship and proved to be an inspiration.

Thanks to my flat mates and friends for their tolerance of my unreliable schedule, and remaining friends throughout the ups and downs of this project. I would also like to thank both my parents, who have directly assisted with this project through discussion, suggestion, and patient reading of my work, but more importantly they have supported me as they always do.

Finally my thanks go out to the Maurice and Phyllis Paykel trust who have directly funded my year, CureKids who support our laboratory, and to all the families who willingly participated in this research showing a great commitment to scientific endeavour.

Table of Contents

List of Figures

List of Tables

Abbreviations

Ala	Alanine
APC	Adenomatous polyposis coli
bp	Base pairs
BSA	Bovine serum albumin
Ca^{2+}	Calcium ions
cDNA	Complementary DNA
CIP	Alkaline phosphatase, calf intestine
CK1	Casein kinase 1
CO_2	Carbon dioxide
DAAM	Dishevelled associated activator of morphogenesis
DEP	Region of DVL – Dishevelled, agl-10, Pleckstrin
DIX	Region of DVL – Dishevelled-Axin
DMEM	Dulbecco's modified eagle media
DMSO	Dimethyl sulfoxide
DNA	Deoxyribonucleic acids
dNTP	Deoxynucleotide triphosphates
droc	Rho-associated protein kinase (*Drosophila*)
DVL, Dvl, dsh	Dishevelled (across a number of species)
DXA	Duel-energy X-ray absorptiometry
EGFP	Enhanced green fluorescent protein
E. coli	*Escherichia coli*
Fz	Frizzled
g	grams
Gly	Glycine
GSK3	Glycogen synthase kinase 3
GTP	Guanine triphosphate
h	Hours

His	Histidine
HSD	Honest significant difference
JNK	c-Jun N-terminal kinase
kb	Kilobase pairs
L	litres
LB	Lysogeny broth media
LEF	Lymphoid enhancer-binding factor
LRP	Lipoprotein related peptide
M	Molar
Mg^{2+}	Magnesium ions
min	Minutes
mL	Millilitres
mRNA	Messenger ribonucleic acid
mtDVL1	The mutant DVL1 construct
NCBI	National Center for Biotechnological Information
NEB	New England Biolabs
ng	Nanogram
nm	nanometres
nmol	Nanomoles
PAGE	Polyacrylamide gel electrophoresis
PAR1	Protease activated receptor 1
PBS	Phosphate buffered solution
PCP	Planar cell polarity
PCR	Polymerase chain reaction
PDZ	Region of DVL – Postsynaptic density 95, discs large, Zonula occludens-1
Pro	Proline
Rac	Ras-related C3 botulinum toxin substrate
Rcf	Relative centrifugal force

RhoA	Ras homologue gene family, member A
RNA	Ribonucleic acid
ROCK	Rho-associated protein kinase (human)
ROR2	Orphan tyrosine kinase receptor 2
RS	Robinow Syndrome
RS-OS	Robinow Syndrome – Osteosclerotic Subtype
s	Seconds
SDS	Sodium dodecyl sulphate
Ser	Serine
shDVL1	The truncated DVL1 construct
TCF	T-cell factor
Tris	Tris hydroxymethyl aminomethane
Thr	Threonine
Trp	Tryptophan
U	Enzyme units
UV	Ultraviolet
wtDVL1	The wild type DVL1 construct
µg	Microgram
µL	Microlitre
µM	Micromolar

Standard nomenclature has been used for gene and gene product identification (from HUGO Gene Nomenclature Committee). As such genes are italicised and the protein products are not (e.g. *DVL1* to DVL1). Human genes/proteins are written all in capitals (e.g. *DVL1*) whereas murine genes/proteins have only the first letter capitalised (e.g. *Dvl1*). *Drosophila* genes/proteins are all lower case (e.g. *dsh* – which is the three letter name for fly Dishevelled).

1. CHAPTER ONE - INTRODUCTION

1.1. Overview of thesis structure

This project largely took place within the laboratory, however there was a strong clinical element to the work shown here.

The Introduction will firstly detail Robinow Syndrome (RS), with a particular focus on the genetic and skeletal aspects of this disorder as these are directly relevant to this thesis. Some forms of RS are caused by loss-of-function mutations in WNT signalling mediators, and this work establishes mutations affecting a previously unassociated component of the WNT pathways, *DVL1* (Dishevelled-1), as causative of RS. These individuals also show osteosclerosis, which is atypical in RS, but reminiscent of the gain-of-function WNT-related osteosclerotic phenotypes. It is this osteosclerotic phenotype, due to its possible gain-of-function mechanism, that is the focus of this project. The second part of the Introduction will review WNT signalling, with a particular focus on its involvement in skeletogenesis. The last component of the Introduction is a focused overview of *DVL1*, the gene central to this work. Chapter 2 provides the clinical analysis of the three cases. The clinical phenotype is important as it drove the hypothesis-based laboratory analysis that is contained in the subsequent chapters. Chapter 3-6 contain the laboratory-based work, firstly Methods (Chapter 3), then endogenous *DVL1* expression (Chapter 4), transfected *DVL1* expression (Chapter 5), and the effect of *DVL1* transfection on canonical WNT signalling (Chapter 6). The clinical and laboratory results are discussed in Chapter 7.

This work has generated two papers, which have been included in the appendices. The first, a clinical description of this RS-OS (Robinow Syndrome –

Osteosclerotic type) was published in the first half of the year (in the *American Journal of Medical Genetics part A,* ref. 1) – some of the research was carried out during a Summer Studentship but the work was completed in the course of this BMedSc. The second is currently in review at the *American Journal of Human Genetics* and it discusses the nature of the *DVL1* mutations in these cases, as well as the impact this mutant protein has on the canonical WNT signalling pathway.

1.2. Value of studying rare syndromes

The investigation of rare genetic pathologies can illuminate the molecular nature of normal physiology and, in future, provide insights into new therapies and treatments for common morbidities. The study of rare Mendelian disorders has been revolutionised by next generation sequencing technology, which has allowed the efficient identification of the genetic aetiology of rare conditions. In turn the identification of the DNA-level aetiology allows focussed functional studies at the protein level giving insights into the signalling pathways active within a cell.

Bone biology has particularly benefitted from the study of rare phenotypes. In 1955 Van Buchem identified a rare recessive sclerosing bone dysplasia that now bears his name (Van Buchem's Disease).[2] In 2002 a genetic analysis of a family with Van Buchem's disease identified a mutation in the gene, SOST, which encodes the protein Sclerostin as causative of this condition.[3] The identification of this gene was instrumental in future work outlining its function, which is to reduce catabolic bone metabolism by inhibiting an aspect of the WNT signalling pathway.[4,5] The therapeutic implications for an identification of a mediator responsible for reducing bone mass are substantial, and currently Sclerostin

antibodies (trade named Blosozumab and Romosozumab) are approaching the end of clinical trials for their use in osteoporosis. An insight from a rare disorder may lead to the treatment of one of the most common and debilitating health conditions.

1.3. The Robinow Syndrome

Robinow Syndrome is a rare genetic disorder first described by the eponymous Robinow in 1969[6] as a new form of dwarfism. There are just over 100 cases from throughout the world of RS reported in the literature. The prevalence is equal between the sexes. RS is traditionally characterised by mesomelic dysplasia, hypoplastic genitalia, and a characteristic facial gestalt often referred to as "fetal facies" (most notably features are hypertelorism, broad mouth, midface hypoplasia, and a wide and depressed nasal bridge). Robinow's initial family showed a dominant inheritance pattern, but a recessive variant of RS was identified in 1978, and initially termed Covesdem Syndrome.[7,8] This recessive RS is again characterised by the above findings, but is generally more severe, with costovertebral segmentation defects such as rib fusions and hemivertebrae (the origin of the original name). Since its identification the recognised clinical phenotype of RS has become increasingly diverse, with heart defects, deafness, oral abnormalities, developmental delay, and a plethora of other deficits being linked to the disorder. The "fetal facies" with the marked hypertelorism is the clearest diagnostic feature of RS, with other defects occurring with varying severity (see ref. 9 for a comprehensive review of the findings of RS, the common signs are presented in Table 1.1 modified and reproduced with permission from the same ref.).

Table 1.1. Features of Robinow Syndrome.
The table shows the frequencies of the common features of dominant and recessive RS. It is reproduced, with permission, from ref. 9. The table has been modified to exclude features with frequencies of less than 50% in both forms.

Characteristic	Prevalence in Dominant RS (%)	Prevalence in Recessive RS (%)
Hypertelorism	100	100
Anteverted mares	96	96
Wide nasal bridge	97	95
Micropenis	84	100
Upturned nose	87	97
Mesomelic limb shortening	80	100
Short stature	81	97
Midface hypoplasia	81	94
Short nose	81	93
Brachydactyly	81	91
Down-slanted mouth corners	63	95
Clinodactyly	70	88
Prominent forehead	79	77
Triangular mouth	65	86
Short hands	62	84
Dental malocclusion	49	94
Cryptorchidism	72	67
Hypoplastic labia minora	50	81
Depressed nasal bridge	78	49
Hypoplastic clitoris	46	80
Micrognathia	57	68
Hemivertebrae	23	98
Long eyelashes	54	59
Gum hyperplasia	36	71
Long philtrum	65	39
Bifid tongue	39	59
Scoliosis	18	77
Macrocephaly	64	26
Highly arched palate	52	14

1.3.1. Robinow Syndrome and skeletal patterning

RS was initially classified as a mesomelic form of dwarfism, however in dominant RS mesomelia is not always present.[10] Recessive RS shows a far greater degree of patterning abnormality, with segmental defects such as rib fusions and hemivertebrae rarely observed in dominant RS.[9] Brachydactyly, notably with hypoplasia of the distal phalanx of the hands and feet, with a bifid thumb and great toe, is a common feature of RS.[11]

1.3.2. Robinow Syndrome and osteosclerosis

RS, as previously discussed, is a heterogeneous disorder with a great variety of features associated with it, however, there are only two previous reports of osteosclerosis. One reports a father-to-son transmission of RS where the father has generalised osteosclerosis and the infant son does not.[12] The second is a sporadic case with osteosclerosis of the mastoids.[13] None of these individuals have segmentation defects, and, when the inheritance pattern is also considered (vertical transmission and sporadic), it is likely that these cases are of dominant RS. These cases are discussed in more detail in Chapter 2.

1.3.3. Genetics of Robinow Syndrome

As well as the clinical diversity RS is also genetically heterogeneous. Recessive RS has been genetically defined by mutations in the gene encoding the orphan tyrosine kinase receptor, ROR2.[14,15] The mutations in *ROR2* are biochemically interesting as another disorder, the dominant brachydactyly type B, is caused by a different set of *ROR2* mutations.[16] The mutations that cause BDB are all truncating, affect the intracellular domain of ROR2[16,17] and are predicted to lead to a dominant negative gain-of-function. In contrast those in recessive RS are

more likely to act through a loss-of-function (a review comparing the mutations in these two disorders is available at ref. 18). Mechanistically it has been shown that recessive RS causing variants lead to a protein that accumulates and is degraded in the endoplasmic reticulum, making the mutations null alleles.[19] Mutations in *WNT5A*, which encodes the typical binding partner of ROR2, are found in some individuals with dominant RS, but these are not present in all cases.[20] There are no other genes previously associated with RS, but our work has established an additional gene, *DVL1*, which is associated with a distinct sub-phenotype of dominant RS. Critically *ROR2*, *WNT5A*, and *DVL1* are all mediators of the WNT signalling pathways (discussed in section 1.4), so while the defects show locus heterogeneity they are linked functionally through a common pathway.

1.3.4. Mouse models of Robinow Syndrome

There are three mouse models of human Robinow Syndrome. As in humans homozygous knockout of *Ror2* leads to a RS phenotype in mice,[21] as does a homozygous knockout of *Wnt5a*.[20,22] Additionally null and hypomorphic alleles of *Prickle1* (a component of the WNT signalling cascade) lead to an RS phenotype in mice,[23] but defects in human homologue, *PRICKLE1*, have not been identified in human RS. *PRICKLE1* variants are, however, associated with human cleft palate,[24] a dysmorphic feature that occurs in RS.

While mice are not used within this work there are a number of reasons why these models are relevant. Firstly the mouse models deepen the understanding of the pathway responsible for RS. For example the *Prickle1* knockouts provide evidence for the potential role of *Prickle1* in RS. Secondly the observation that

mice will phenocopy RS adds confidence to subsequent discussion surrounding the non-RS phenotype of homozygous knockouts of *Dvl1* in mice.[25]

1.4. WNT signalling pathways

WNTs are a diverse family of lipophilic cysteine rich extra-cellular signalling molecules, which give rise to numerous intracellular responses. WNT signalling regulates a great range of processes including, but by no means limited to, skeletal patterning, bone mass, and mechanosensing. WNTs are often considered 'morphogens' – long-range signals that act in a concentration dependent manner, and they are of particular importance during development. WNTs are produced and expressed ubiquitously during development and throughout an organism's life (WNT signalling is reviewed in refs. 26, 27, and 28).

The name 'WNT' is derived from a contraction of Wingless and Insertion, documenting the history of its discovery.[29] Broadly there are three intracellular WNT signalling pathways: the canonical/β-catenin dependent pathway, and the non-canonical pathways, further divided into the WNT/Ca^{2+} and WNT/PCP signalling pathways. This chapter will discuss the basic mechanisms and effects of these pathways in bone with a particular focus on DVL1. At the end of this section Figure 1.1 presents an overview of WNT signalling.

1.4.1. WNT agonists and antagonists

There are 19 extracellular WNTs (the classical WNT ligand) in humans. Dividing these ligands into canonical and non-canonical agonists is difficult as the nature of the receptors expressed on the responding cell influence the downstream

signals triggered by any given WNT.[30] However in normal physiological conditions WNT1, WNT3A, and WNT8 can be considered canonical WNT agonists, where as WNT5A and WNT11 preferentially mediate non-canonical activation (reviewed in ref. 27).

There are now known to be other, non-WNT, extracellular proteins that also activate the WNT pathway including Norrin[31] and proteins in the R-spondin family.[32] Both of these activate the β-catenin pathway. For clarity this chapter will refer simply to WNT agonists as "WNTs" as this work does not differentiate between canonical WNT agonists.

There are a number of WNT antagonists but only a few are relevant to this work. Firstly the non-canonical WNT pathways will inhibit the β-catenin dependent pathway. The precise mechanism of this is unclear but it occurs downstream of canonical β-catenin stabilisation[30] (pictured in Figure 1.1 as a dotted line). Secondly the gene *SOST* (discussed previously) encodes the extracellular protein Sclerostin that will inhibit canonical WNT signalling via an interaction with the Lipoprotein Related Peptides (LRPs).[5]

1.4.2. Canonical/β-catenin WNT pathway

This was the first WNT pathway identified and it remains the best understood. An interaction between a WNT, the Frizzled (Fz) receptor, and an LRP co-receptor initiates the molecular cascade culminating in β-catenin accumulation and translocation to the nucleus which activates transcription factors, most notably T cell factor (TCF) and lymphoid enhancer-binding factor (LEF). The WNT/Fz/LRP complex interacts with DVL and Axin. Axin in turn acts as a scaffold directly binding to DVL, Caseine Kinase 1 (CK1), Glycogen Synthase

Kinase 3 (GSK3), and APC (adenomatous polyposis coli). Unbound CK1, GSK3, and APC form a destruction complex which phosphorylates β-catenin, in turn promoting its ubiquitination and degradation. The WNT mediated interaction of this complex with Axin de-activates the destruction complex. Thus, in the presence of WNT, cytoplasmic β-catenin accumulates and subsequently translocates to the nucleus where it interacts with the aforementioned transcription factors (see ref 26 for a detailed review).

DVL polymerisation is an important step in canonical signalling. It is well documented that DVL will form cytoplasmic puncta, which have been shown not to be associated with vesicles, being instead polymers of DVL.[33] The formation of these dynamic DVL polymers acts as an unusual regulatory mechanism. The local accumulation of DVL, driven by the formation of polymers, facilitates canonical WNT signalling by concentrating DVL sites which then interact with downstream WNT mediators.[34] There is evidence that DVL also plays a role within the nucleus in canonical WNT signalling. The disruption of the nuclear import signal in dsh (fly DVL) abrogates its ability to signal in the canonical WNT pathway in transfected mammalian cells.[35]

1.4.3. PCP/WNT signalling

This aspect of WNT signalling is primarily considered to control the convergent extension movements of gastrulation during embryogenesis.[27] The pathway is similar to the Planar Cell Polarity (PCP) pathway in *Drosophila* (reviewed in ref. 36), hence the name. There is some debate regarding which aspects of WNT signalling are encompassed by PCP/WNT but this work will use the term PCP to describe the non-β-catenin, non-Ca^{2+} mediated aspects of WNT signalling.

WNT5A is the archetypal activator of non-canonical WNT signalling. A phenotypic similarity between WNT5A$^{-/-}$ mice and knockouts of the Orphan Tyrosine Kinase Receptor 2 (ROR2$^{-/-}$) mice led to the identification of the transmembrane ROR2 as a receptor for WNT5A. ROR2 will associate with the traditionally non-canonical Fz receptors Fz2 and Fz5, to act as a WNT co-receptor.[30]

PCP signalling begins with an interaction between WNT5A and ROR2 either acting alone or as a co-receptor with an appropriate Fz. This initial interaction leads to the polarisation of a Fz-DVL-Diversin proximal to the signal and Prickle-Vangl distally, thus establishing a polarity across the axis of the cell (discussed in refs. 37 and in 38).

DVL, subsequent to this polarisation, interacts with a GTP-binding protein, RhoA, via DAAM1.[39] Work in *Drosophila* showed that the DVL-activated GTP-bound RhoA will interact with Drok (ROCK in humans) which affects actin polymerisation via the non-muscle myosin regulatory light chain phosphorylation of myosin II.[40]

DVL will also activate another small GTP-binding protein, Rac, which will in turn activate c-Jun N-terminal kinase (JNK), which influences the actin cytoskeleton and gene transcription. The mechanism for this DVL-Rac interaction is still unknown.[41] There is some debate as to whether this part of PCP signalling should be grouped with WNT5A/ROR2 signalling, as ROR2 may not be required to activate JNK nor to inhibit β-catenin signalling.[42]

As discussed above non-canonical WNT signalling inhibits canonical WNT signalling through an unknown mechanism downstream of the β-catenin stabilisation[30] (this thesis has grouped this action with the PCP/WNT pathway). Interestingly, as PCP/WNT is based on the establishment of polarity, both over and under expression of PCP/WNT components can lead to the same phenotype.[43] This is an indication that some PCP/WNT mutations may be better considered as 'disruptive to' PCP/WNT signalling rather than the simple binary notion of a loss- or gain-of-function.

1.4.4. Calcium signalling and DVL

Initial over expression experiments in zebrafish blastulae showed that *WNT5A* or *Fz2* increased the frequency of calcium influxes.[44,45] The WNT-Fz interaction activates heterotrimeric G-proteins which in turn activate phospholipase C. This stimulates inositol-1,4,5-trisphosphate production, which triggers the release of Ca^{2+} from intracellular stores. The role and mechanisms of the Ca^{2+}/WNT pathway is reviewed more comprehensively in ref. 46.

The precise role of DVL in this Ca^{2+} response is very complex. Early work showed that over-expressing a DVL construct that lacked a specific domain called DIX (discussed in a section 1.5.2) would lead to a pertussis toxin insensitive (i.e. not G-protein dependent) increase in the frequency of Ca^{2+} influxes. In contrast over-expressing full length DVL led to a milder increase in Ca^{2+} influxes.[47] The insensitivity to pertussis toxin led the authors to conclude that either DVL was acting downstream or in parallel to the G-protein mediated response. A more recent study used fluorescently tagged constructs and live cell imaging to observe the DVL-Fz-G-protein interactions in real time. This work argued for a

complex of all three molecules in the initiation of the Ca^{2+} response. DVL, in this complex, had an enigmatic regulatory function where both its over- and under-expression would interfere with the complex formation and abrogate the WNT induced Ca^{2+} response.[48] The DIX domain was identified as inhibiting the Fz-G-protein association,[48] which is consistent with the findings discussed above.[47] Taken together these results may indicate that DVL has dual roles: both regulating the Fz-G-protein mediated calcium signalling, and promoting calcium signalling either down stream or in parallel to G-proteins (shown with a dotted line in Figure 1.1).

1.4.5. WNT signalling in bone metabolism and skeletal disease

The role of WNT signalling in bone metabolism is well established (see 49 for a comprehensive review). In broad terms the canonical pathway is associated with regulation of bone mass, the PCP pathway with skeletal patterning, and the calcium dependent signalling is involved in some aspects of mechanosensing.

The canonical WNT pathway is strongly associated with the regulation of bone mass. Mutations in *SOST*, the secreted WNT antagonist, will cause Van Buchem's and Sclerostosis – conditions of markedly increased bone mass.[3,50] Gain-of-function mutations in *LRP5*, an activator of canonical signalling, will also cause a high bone mass phenotype.[51] Conversely both heterozygous and homozygous loss-of-function mutations in LRP5 will cause osteoporosis.[52,53,54] Additionally an *LRP4* haplotype has been associated with low bone mineral density in genome-wide association studies[55] and mouse knockouts of genes encoding the canonical agonists WNT3A, LRP4, 5, and 6 are associated with low bone mass (reviewed in 49).

The PCP/WNT pathway mediates skeletal patterning rather than bone mineral accrual. Loss-of-function mutations in the PCP/WNT components *WNT5A* and *ROR2* will cause dominant and recessive RS respectively.[14,15,20] Different mutations in *ROR2* cause the severe brachydactylic type B, another skeletal patterning defect.[16] *Prickle1*, a PCP mediator, will cause an RS phenotype in mice when knocked out[23] and common and rare variants in *PRICKLE1* are associated with cleft palate in humans.[24] Interestingly *WNT5A* knockdown is also associated with a low bone mass phenotype in mice through an impact on osteoblastogenesis, as WNT5A potentiates osteoblastogenesis over adipogenesis in differentiating mesenchymal stem cells.[56] As discussed in section 1.4 PCP/WNT regulates convergent-extension movements in embryogenesis, therefore defects in PCP/WNT components cause convergent-extension dependent phenotypes in humans: such as the aforementioned cleft palate and neural tube defects. A number of variants in PCP/WNT mediators have been found to associate with neural tube defects in humans, these include, amongst others: *VANGL1*[57] and *2*;[58] *PRICKLE1*;[59] *FRIZZLED6*;[60] and DVL2[61] (these are reviewed in ref. [62]).

The role of the WNT/Ca^{2+} in bone is less well defined, but it is involved in the remodelling associated with mechanical stress, effecting both osteoblasts and osteoclasts.[63,64]

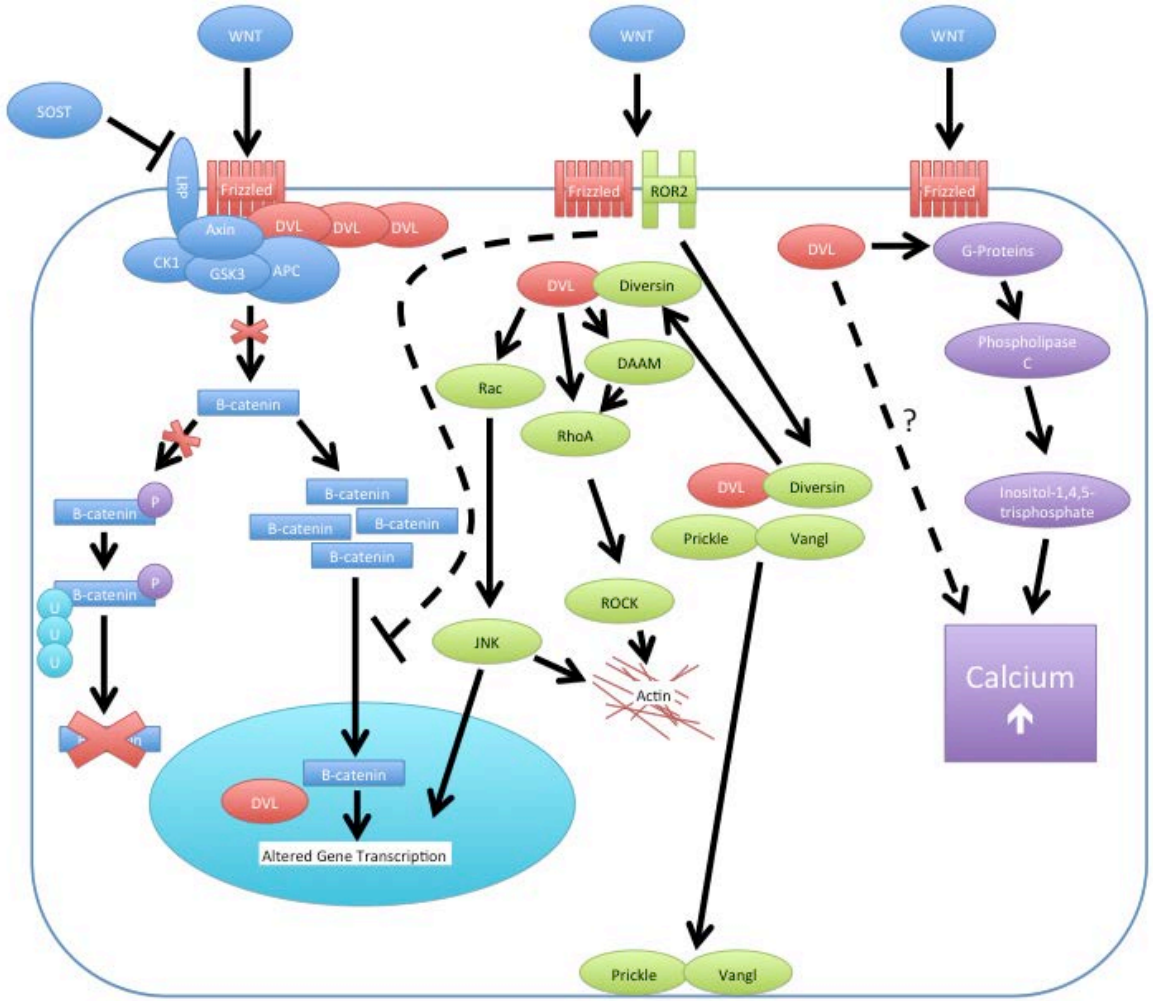

Figure 1.1. An overview of WNT signalling
Note the three WNT cascades, which are, from left to right: the canonical/β-catenin, the PCP/WNT, and the Ca^{2+}/WNT pathways. DVL is marked in red. In response to WNT stimulus, in the canonical cascade, the DVL dynamic DVL polymer interacts with the β-catenin destruction complex, which stops phosphorylating β-catenin. β-catenin, when unphosphorylated, is not ubiquitinated and degraded, thus it accumulates within the cytoplasm and translocates to the nucleus where it alters gene transcript through interactions with transcription factors (notably LEF and TCF) and DVL. In the PCP pathway WNT stimulus acts via ROR2/Fz to cause DVL and Diversin to polarize to the proximal pole of the cell and Prickle and Vangl to move to the distal pole. DVL then interacts with Rac and RhoA which activate JNK and ROCK respectively. Both ROCK and JNK influence the actin cytoskeleton and JNK also alters gene transcription. The mechanism by which the PCP inhibits the canonical pathway is unknown. In the Ca^{2+}/WNT DVL acts in parallel to and directly with a G-protein initiated cascade that culminates in an increase in the intracellular calcium levels. This figure was drawn on the basis of the references contained in section 1.4.

1.5. Dishevelled

Dishevelled was originally identified in *Drosophila* (in which it is know as *dsh*) and its name derives from the disruption in bristle and hair polarity caused by its mutation.[65] *Drosophila* has one isoform of Dishevelled, whereas mammals have three (*DVL1*, *2*, and *3* in humans), however the basic structure of each DVL is strongly conserved across the paralogues and they all show a close resemblance to fly *dsh*.[66] As discussed previously DVLs are WNT mediators that act across all known WNT pathways (see Figure 1.1). Often they are described as "scaffold-like" proteins, acting directly downstream of the transmembrane WNT receptor (generally a Fz, but sometimes an LRP or ROR2). Most mammalian DVL is DVL2, making up over 90% of the cellular DVL.[67] However DVL1 and 3 (only ~5% each) have a greater impact upon canonical WNT signalling when knocked down than DVL2.[67]

1.5.1. *DVL1* gene structure

DVL1 is a 15-exon gene located in the short arm of chromosome 1 in humans. The top panel of Figure 1.2 shows *DVL1* gene structure. The three mutations discussed in this thesis occur in the 14th exon.

1.5.2. Regions of DVL1 protein

All DVLs have the same three conserved regions, which, from N-terminal to C-terminal, are: the DIX (Dishevelled, Axin); the PDZ (Postsynaptic density 95, Discs Large, Zonula occludens-1); and the DEP (Dishevelled, Agl-10, Pleckstrin). In broad terms the DIX domain is important for DVL's ability to self associate into supramolecular complexes (forming visible puncta), the PDZ allows the transduction of signals from the intramembrane Frizzled receptor, and the DEP

interacts with downstream mediators of WNT signalling (DVL function is reviewed in ref. 37). Between the DIX and PDZ domains is a basic region that is believed to be important for the interaction of kinases with DVL. In particular PAR1 binds to this region,[68] as does Casein Kinase 2.[69,70] There is also a proline rich region between the PDZ and DEP which contains an SH3-binding domain.[71] This proline rich domain has been shown to bind to Src family tyrosine kinases in response to WNT3A stimulus, and the subsequent phosphorylation (driven by the activated kinases) is a necessary step for β-catenin nuclear localisation and TCF/LEF activation (both measures of canonical WNT activation).[72] Of particular interest to this project Src tyrosine kinases also bound to the C-terminal of Dvl2 (residues 511-736), which is broadly homologous to the C-terminal of DVL1.[72] The bottom panel of Figure 1.2 is a cartoon of DVL1 showing the three major regions (approximately to scale) and the location of the basic (B) and proline rich (P) regions. Note the substantial portion of C-terminal protein, it is this region that the mutations affect in the cases of RS studied in this work.

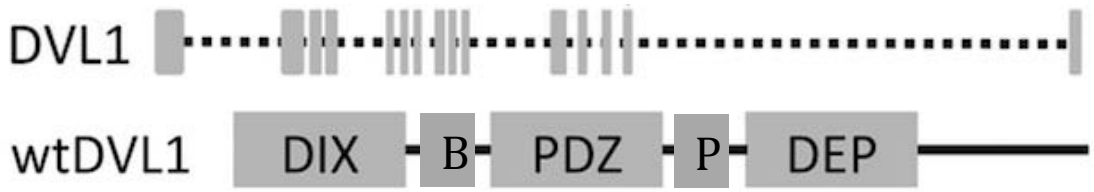

Figure 1.2. DVL1 gene and protein structure.
The top panel shows the exon structure of *DVL1*, which has 15 exons (the 14th is the location of the mutation in the three cases discussed in this project). The panel is a cartoon showing DVL1 protein structure, the length of each region is approximately to scale. Note the elongated C-terminus after the DEP domain. This is the region affected by the frameshift mutations studied in this work.

1.5.3. DVL C-terminus

The DVL C-terminus is one of the more variable parts of the DVL proteins, with DVL3 in particular showing a number of unique residues.[73] Nevertheless the majority of the sequence is still conserved between paralogues (only ~25% of the DVL3 C-terminal is unique to DVL3[74]). The DVL-C-terminal (in some of the work grouped with the DEP domain) contains: critical sites for regulating the phosphorylation of DVL;[75] sites that regulate stability through interactions with ubiquitin ligases[76,77,78] and a degrading enzyme;[79] binding sites for the Src tyrosine kinases discussed above;[72] a Frizzled binding domain;[80] sequences involved in nuclear localisation;[81] a binding site of a deubiquitinating enzyme;[82] and a region that interacts with ROR2.[83] More detail on the C-terminal interacting proteins is found in the Discussion, in the context of the findings of this project.

1.5.4. Dvl mouse knockouts

There are three Dishevelleds in mammals and the overlapping but distinct roles of each *Dvl* (murine) have been elegantly shown in a series of mouse knockouts.[84] *Dvl1* null mice display no physical phenotype, however they do have some social abnormalities.[25] 50% of *Dvl2* null mice die at birth and the remainder show severe defects in patterning. In particular these are cardiac, neural tube, and segmentation defects.[85] *Dvl3* null mice will rarely survive until adulthood and have a similar phenotype to the *Dvl2* nulls, but also show cochlear defects with the abnormal alignment of hair cells.[86] Demonstrating the overlapping roles, through a more severe phenotype, 100% of *Dvl1*/*Dvl2* double knockouts have a completely open neural tube and exencephaly as well as

cochlear defects similar to those found in the Dvl3 nulls.[87] *Dvl1*/*Dvl3* double knockouts are embryonic lethal but without neural tube defects suggesting a distinct role for *Dvl2* in this respect.[86] *Dvl2*/*Dvl3* nulls have never been observed, suggesting early lethality.[86] Transgenes under the control of the native promoters of other *Dvls* can rescue the lethal phenotypes caused by knockouts. For example a *Dvl1* transgene could rescue the lethality of *Dvl3*$^{-/-}$ but not that of *Dvl2*$^{-/-}$, however a *Dvl3* transgene was able to rescue the *Dvl2* double knockout.[84] This again demonstrates the overlapping (and perhaps redundant) roles of the DVLs.

In summary the following conclusions can be drawn from the mouse models: *Dvls* have both overlapping and distinct functions; *Dvl1* knockout has the least impact upon phenotype; and no single or combination of *Dvl* knockouts led to an osteosclerotic or RS phenotype, as was observed in the human cases studied in this thesis.

1.5.5. The distinct roles of Dvl paralogs in WNT/Ca^{2+} signalling

In contrast to the apparent redundancy discussed above, a study in isolated mouse embryonic cells found that the knockdown of any of the *Dvl* paralogues repressed the WNT5A-Ca^{2+} response. Each Dvl did this to a similar degree despite the fact that Dvl1 and Dvl3 make up a substantially smaller part of the total DVL pool. It was also found that neither *Dvl1* nor *Dvl2* over-expression could rescue the *Dvl3* knockdown induced reduction in Ca^{2+} response.[73] The role of Ca^{2+} falls largely outside the scope of this project, and, while the results discussed here are themselves compelling they do not sit comfortably with the substantial overlap in function demonstrated in the whole organism mouse

work. Given the almost complete absence of phenotype in the *Dvl1*$^{-/-}$ mouse two explanations present themselves: either Ca^{2+}/WNT signalling via *Dvl1* is of relatively little systemic importance, or in the whole mouse there is some compensatory mechanism that rescues function (which was not accounted for in the cell culture-based assay).

1.5.6. DVL in Human Disease

Until this work *DVL* mutations have been large not associated with a WNT-related phenotypes in humans. *DVL2* and *DVL3* are not, to our knowledge, associated with human disease (excepting the two *DVL2* variants in two cases of neural tube defects,[61] see section 1.4.5). Monosomy 1p36 Deletion Syndrome, a disorder characterised by dysmorphism and mental retardation may conceivably be contributed to by a haploinsufficiency of *DVL1*. *DVL1* sits in the region deleted in this syndrome,[88] but as do many another of other genes.[89,90,91] Critically these individuals do not have RS or osteosclerosis, nor do individuals with other chromosomal deletions of the region containing *DVL1*.[92]

1.6. Summary of literature

RS is a diverse clinical entity, which is divided on the basis of inheritance patterns into dominant and recessive forms. The phenotypes of the milder dominant and more severe recessive forms overlap but are distinct – severe segmentation defects occur almost exclusively in the latter. RS can be caused by loss-of-function defects in *ROR2* and *WNT5A*, which are genes involved in PCP/WNT signalling: a pathway primarily associated with skeletal patterning and convergent extension. *DVL1*, the focus of this project, is also a component of the PCP/WNT pathway, but, until this work, has not been associated with RS. The

three affected individuals discussed in this thesis have a phenotype that combines RS with osteosclerosis (RS-OS).

It is the osteosclerotic aspect of this phenotype which is the focus of this thesis, it was preferentially studied over the RS component for three reasons. Firstly loss-of-function mutations in PCP/WNT mediators are associated with RS and gain-of-function mutations in canonical WNT mediators are linked to osteosclerosis. From a biochemical perspective gain-of-function mutations are more interesting than the simpler loss-of-function. Secondly it is the osteosclerosis that differentiates these individuals from other RS cases, thus this new feature was of more immediate interest. Thirdly there are practical constraints regarding the study of PCP/WNT signalling which are detailed in the Discussion.

1.7. Aims of Study

This project was initiated by the identification of two cases of a novel disorder, termed RS-OS (work in review at the *American Journal of Human Genetics*), which shared a common genetic observation: *de novo* frame shift mutations in the 3' end of the gene *DVL1*. This project has two broad aims. The first is to clinically define this disorder and search for additional cases in the literature. The second aim was to characterise the functional implications of these mutations, initially investigating the transcription and translation of the mutant alleles and subsequently determining the impact on the canonical WNT signalling pathway through transient transfection-based TOPFlash assays.

2. CHAPTER TWO – CLINICAL ANALYSIS

2.1. Strategy

RS, as discussed in the introduction, is a widely heterogeneous disorder. This section of the project aimed to clinically characterise this osteosclerotic subtype of RS (RS-OS). Given the shared genetic aetiology across these three cases, we hypothesise that features beyond just the osteosclerosis may define this subtype of RS. However, as RS itself is so heterogeneous, describing unique features to these cases is essentially impossible (excluding the osteosclerosis). Additionally it is plausible that some cases in the literature may in fact belong to the subtype RS-OS, since without detailed x-rays the osteosclerosis could easily be missed. As such this section attempts to draw out aspects that are rare in RS but relatively consistent across the individuals with RS-OS, perhaps indicating the features distinct to this subtype. A number of cases are also drawn from the literature, while there is no way to test the genetics of these individuals the presence of osteosclerosis could well be an indication that they fit our subtype.

Some of the research in this section was carried out during a Summer Studentship, however the majority of the work occurred during this BMedSc.

2.2. Clinical Methods

My supervisor (Stephen Robertson) identified Case 1 during his clinical practice. Angeline Lai (a collaborator from KK Women's and Children's Hospital, Singapore) identified Case 2. Case 3 was originally published by Eijkenboom *et al*[93] and identified by the distinct clinical features during my research into RS-OS. The information from Case 1 was gathered through clinical examination and interview (conducted by myself and Stephen Robertson), and studying hospital

records. For Case 2 we examined clinical images and radiographs sent to us and used the information from a clinical examination and hospital records provided by Angeline Lai. We were also able to gather additional information when we interviewed Case 2 and their family during a visit to New Zealand at the end of 2014. Sue Craw (Department of Radiology, Dunedin Hospital) assisted our interpretation of the radiographic findings from Cases 1 and 2. Information from Case 3 was gained by correspondence with Henricus Kunst (Radboud University Medical Center, Nijmegen, the Netherlands) and directly from the paper published by Eijkenboom *et al*.[93] I have carried out a review of the RS literature, and it is this that identified Case 3 and allowed the characterisation of this RS-OS subtype and the identification of the other possible earlier cases (Cases 4-6).

2.3. Case 1

This female was born at term to non-consanguineous parents aged 31 (maternal) and 42 (paternal). A bi-lobed and hypomobile tongue, hypoplastic uvula, short nose, and wide mouth were observed at birth. In the hands camptodactyly, clinodactyly, and brachydactyly were present. In childhood she developed chronic otitis media (which was treated twice with grommets) and recurrent chest infections. All primary teeth failed to exfoliate and had to be surgically extracted, after which she was found to be oligodontic with the agenesis of 12 secondary teeth.

At the age of 13 she was 147.8cm tall (-1.25 SD) and weighed 40kg (-0.7 SD) with a head circumference of 60cm (>+2 SD) She had marked hypertelorism (intercanthal distance 4cm, >+2 SD), wide and depressed nasal bridge, short nose, and excessive anterior lower facial height (see Figure 2.1 for phenotype).

Pectus carinatum was observed. Additional to the oligodontia there was marked gingival hypertrophy, moderate tooth crowding, and severe mesial rotation of the upper left incisor.

Figure 2.1. Clinical appearance of Case 1.
This figure is reproduced from the clinical paper in the appendix of this work (ref. 1), it shows Case 1 at 16 years of age. A and B, the distinctive facial appearance with hypertelorism, wide and depressed nasal bridge, and midface hypoplasia. C and D, the hands a feet showing the brachydactyly, clinodactyly, and camptodactyly.

At 16 years old radiographs revealed a marked generalised osteosclerosis, particularly observable at the base of the skull. The frontal sinuses were hypoplastic, the long bones undertubulated, and the ulna bilaterally bowed. The distal phalanges of the hands and feet were hypoplastic and the distal phalanx of the great toe and thumb were bilaterally bifid (Figure 2.2). Aside from the osteosclerosis the vertebral axial skeletal morphology was unremarkable, showing no rib fusions or hemivertebrae. She had bilateral mixed hearing loss. Dual-energy X-ray absorptiometry (DXA) found an average bone density of 1.584g/cm^3 (Z-score, which is an age and sex matched standard deviation, +5.9), and the lumbar density was 1.960g/cm^3 (Z-score +5.9). At 21 years her height

was 159.3cm (25th centile) and a DXA scan found a relative and absolute rise in bone density to such that her lumbar vertebral density was now 2.08g/cm^3 (Z-score +7.4). Notably, mesomelia was absent. There was no history of pathological fractures.

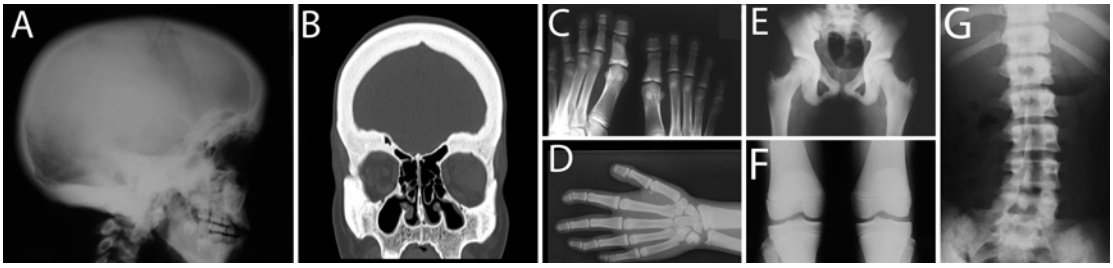

Figure 2.2. Radiographic appearance of Case 1.
This figure is reproduced from the clinical paper attached in the appendix (ref. 1). The images were taken at 16 years of age. A and B show the dramatic osteosclerosis of the cranial vault particularly clear in the base of the radiograph (A) and the hyperdensity and thickness of the bone in the coronal CT (B). C and D show the left hand and feet with osteosclerosis, brachydactyly, clinodactyly, camptodactyly as well as the bifid thumb and great toe. E-G, note the generalized osteosclerosis, lack of segmentation defects, and the undertubulation of the long bones in F.

These features (no rib fusions, mesomelia, or hemivertebrae) and the lack of parental consanguinity support a diagnosis of dominant, rather than recessive, RS.[9] The common features of dominant RS present in this case (compared to the review in ref. 9, over 50% occurrence in dominant RS was considered common) are: hypertelorism, midface hypoplasia, short nose, wide and depressed nasal bridge, macrocephaly, clinodactyly, and brachydactlyly.

2.4. Case 2

This male was born at 36 weeks gestation by elective Caesarean section to non-consanguineous parents aged 28 (paternal) and 29 (maternal). Antenatal scans were normal until 6 months gestation when short limbs and increased skull size were noted. A cleft lip and palate, and umbilical herniation were corrected at

birth. Bilateral intra-abdominal testes were treated by left orchidectomy and right orchidopexy.

He was diagnosed with recurrent otitis media in childhood and his primary teeth failed to exfoliate prompting their surgical removal at 11. At 9 years of age weight and height were both above the mean, and the head circumference was 62.7cm +>2 SD). Hypertelorism, a broad nasal root, a flattened nasal tip, and narrow nares were evident. A short tongue, gingival hyperplasia, and tooth crowding were found on oral examination. Brachydactyly, broad thumbs, camptodactyly (Figure 2.3), along with bilateral flat feet were found. There was no history of pathological fractures.

Radiographs showed widespread osteosclerosis most markedly in the base of the skull (Figure 2.3) and cortices of the long bones. The long bones were undertubulated. The distal phalanges of the hands and feet were hypoplastic and terminal phalanx of the thumb was bifid bilaterally. A DXA scan at 11 years of age showed an increased bone mineral density, with an average of 1.264g/cm^3 (Z-score +7.6). Notably some common features of RS (micropenis and mesomelia) were absent.

As in Case 1 the inheritance (sporadic) and the features (no micropenis, hemivertebrae, mesomelia or rib fusions, and presence of umbilical herniation, which is exclusive to dominant RS[9]) indicate dominant RS. Common features of dominant RS in this case (same criteria as Case 1) are: brachydactyly, hypertelorism, macrocephaly, midface hypoplasia, and cryptorchidism.

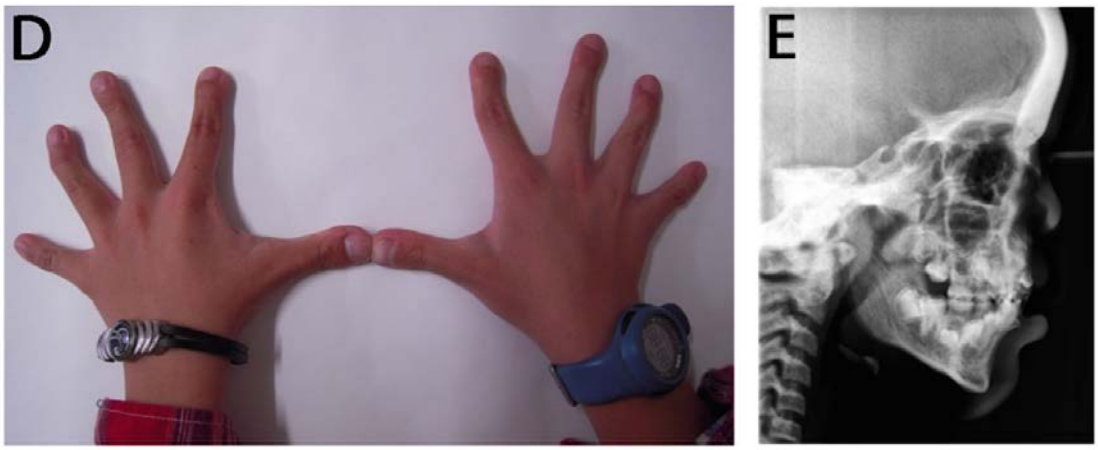

Figure 2.3. Hands and skull of Case 2.
This is a section of a figure from the *American Journal of Human Genetics* paper enclosed in the appendix (in review). It shows that hands of Case 2 with marked brachydactyly and camptodactyly (D) and a lateral radiograph of the skull revealing the osteosclerosis, most noticeable at the skull base (E).

2.5. Case 3

This case was initially documented by Eijkenboom et al.,[93] and while our lab received DNA samples we have had limited additional clinical information. The relevant findings from the paper are summarised, although the clinical detail is sparser than that presented for Cases 1 and 2.

This case was a 17-year-old female, born at full term in an uncomplicated non-consanguineous pregnancy. Dysmorphic facial features, brachymesomelia, intestinal malrotation, umbilical herniation, and mild subvalvular stenosis of the pulmonary artery were noted at birth. Midface hypoplasia, hypertelorism, depressed nasal bridge, prominent forehead, long philtrum, a large and bifid tongue and dental malocclusions with the absence of 2 permanent lateral incisors were observed. She had a history of recurrent airway infections. She had bilateral mixed hearing loss. There was no reported history of pathological fractures.

Osteosclerosis (referred to as hyperostosis in the original paper from Eijkenboom et al.) was found in the skull and in particular the bones of the inner ear by CT scan, which the authors concluded provided an explanation for the hearing loss. To our knowledge no general X-rays were taken and no DXA scan was performed.

Eijkenboom et al. concluded that the clinical diagnosis was one of dominant RS, due to the inheritance pattern (sporadic) and features (umbilical herniation and lack of segmentation defects). The classic facial features of RS and mesomelia are reported in this Case.

2.6. Osteosclerosis previously in Robinow Syndrome

As noted in the Introduction osteosclerosis in RS has been reported twice previous to this work, one in a father-to-son transmission[12] and one sporadic case.[13] Both of these have the features of dominant RS as well as the supporting inheritance pattern (vertical transmission and sporadic). In the sporadic case[13] the osteosclerosis was confined to the mastoids, but in the father-to-son transmission the father showed generalised osteosclerosis.[12]

2.7. Robinow Syndrome with osteosclerosis

It is our hypothesis that the three cases included in this thesis and the further three from the literature represent a distinct sub phenotype of dominant RS with osteosclerosis (RS-OS). As such five of these patients show osteosclerosis, measured either from DXA scans,[1] radiographs,[12,13] or CT scans.[93] We hypothesise that the osteosclerosis is progressive. DXA scans of Case 1, first at 16 then at 21 years-of-age, showed an increase in bone density. The sixth case, the

son of the osteosclerotic father described by Shprintzen et al,[12] does not show osteosclerosis. This would be consistent with a progressive phenotype that was not visible at birth. The progressive nature of the osteosclerosis will only be confirmed by the on-going monitoring of these affected individuals. The following table summarises the notable clinical features of RS-OS. Findings that occur commonly in RS have been omitted (more than 50% prevalence from ref. 9). It is worth noting, however, that the prevalence of some oral features is debated, a substantially smaller study, ref. [94], found that gingival hyperplasia, oligodontia, bifid tongue, cleft lip/palate, and gingival hyperplasia occurred more frequently in dominant RS than found in the larger cohort in ref. 9. This work uses the figures from the larger review, ref. 9, which are also included as a table in the Introduction.

Table 2.1. Clinical features of all reported cases of RS with osteosclerosis.
Features that occur with a frequency of greater than >50% in dominant RS (from ref. 9) have been omitted.

	Age at examination	Bone Mineral Density	Auditory Findings	Oral Findings	Herniation and other	Source
Case 1 - Female	16 and 21 years	General osteosclerosis on radiograph. DEXA scan revealed a lumbar bone density of 1.960g/cm3 (Z-score +5.9) at 16, and 2.08g/cm3 (Z-score +7.4) at 21.	Bilateral mixed hearing loss at 16. Recurrent chronic otitis media.	All primary teeth failed to exfoliate. Absence of 12 secondary teeth. Marked gingival hypertrophy, hypoplastic uvula, and a bi-lobed tongue.	None	Ref. 1
Case 2 – Male	11 years	Radiograph showed generalised osteosclerosis. DXA scan revealed a lumbar bone mineral density of 1.264g/cm3 (Z-score +7.6).	Recurrent chronic otitis media.	All primary teeth failed to exfoliate. Gingival hyperplasia, and a left cleft lip and palate.	Umbilical hernia at birth	Ref. 1
Case 3 – Female	17 years	Information on the general skeleton was not available, and those x-rays (if taken) were unattainable. However osteosclerosis of the skull was documented.	Bilateral mixed hearing loss, recurrent chronic otitis media	Absence of two lateral incisors.	Umbilical hernia at birth, intestinal malrotation, subvalvular stenosis of the pulmonary artery	Ref. [93]
Case 4 – Male	13	Slight general increase in bone density, marked sclerosis of the mastoids	Conductive hearing loss after chronic otitis media	Primary teeth failed to exfoliate. Oligodontia (missing 11 teeth), hypoplastic uvula, gingival hyperplasia	Umbilical hernia	Ref. 13
Case 5 – Male	23	General increase in bone density on radiographs, marked in the skull	None Reported	Bifid uvula and sub mucosal palate cleft, left side cleft lip		Ref. 12
Case 6 – Male	30 months	None	None Reported	Bilateral cleft lip and palate	Umbilical hernia	Ref. 12

2.8. Summary of clinical research

The work outlined in this section has established a clinically distinct entity: RS-OS. This clinical definition, from Cases 1 and 2, was used to identify Case 3 from the literature, whose DNA was sequenced (see Chapter 4) and strengthened the evidence for the causative role of *DVL1* mutations in this disorder. The clinical finding of RS-OS led us to hypothesise that these individuals have disrupted PCP/WNT signalling causing their RS and an over-activity in canonical WNT signalling leading to osteosclerosis (see Introduction). It is largely this hypothesised link to osteosclerosis that is assessed in the remainder of this thesis, for reasons indicated in the Introduction and Discussion.

3. CHAPTER THREE – LABORATORY

MATERIALS AND METHODS

3.1. Outline

This section contains the methods which were used multiple times throughout the lab-based part of this project. More detail on how each method was applied to a specific part of this work is included in the relevant section of the Results.

3.2. Ethical Approval

The Southern Health Research and Disability Ethics Committee approved this work, under the approval number 13/STH/56.

3.3. Cell culture, RNA extraction, and cDNA synthesis

3.3.1. Human fibroblast and C2C12 cell culture

Human fibroblasts, extracted by dermal biopsy, from Case 1 and two unaffected controls were available in the laboratory. These cells were stored in media (described below) containing 5% DMSO (dimethyl sulfoxide) at -80^{o}C. The mouse mesenchymal stem cell line C2C12 was used for the transfection experiments. Cultures were grown in DMEM (Gibco) supplemented with 10% foetal bovine serum (Moregate Biotech, FBSF) and 1% L-glutamine (Gibco, 25030). They were maintained in 5% CO_2 at 37^{o}C. All cells were grown in 25mL or 75mL flasks and passaged at 80-90% confluence as assessed by inverted stage phase contrast microscopy.

3.3.2. Human fibroblast RNA extraction and cDNA synthesis

A confluent 25 mL flask of fibroblasts was trypsinised with 0.5mL of trypsin (Gibco) at 37^{o}C for 3 min, diluted in phosphate buffered solution (PBS), then pelleted by centrifugation at 250 rcf (Eppendorf 5810R). The supernatant was

removed then the pellet processed using the NucleoSpin RNA kit (Macherey Nagel, 740902) according to the manufacturer's protocol with 2-mercaptoethanol added to the lysis buffer. The RNA was quantified using a NanoDrop®1000.

The SuperScript®II kit (Invitrogen 18064) was used for cDNA synthesis. 0.5 µg of RNA was incubated with 0.5 µg of random hexamer primers in 11µL of MilliQ water for 5 min at 65°C. 4 µL of buffer, 4 µL of dNTPs (200 µM), and 1 µL of DTT (0.1 M) was added to the above reaction and incubated at 50°C for 1 h. A reverse transcriptase negative reaction was used to assess DNA contamination. The cDNA was diluted 1:4 in MilliQ water before PCR (polymerase chain reaction), either for mRNA sequencing or restriction digest (both described below).

3.4. PCR and DNA manipulations

3.4.1. Primer design

Primers were designed using the NCBI Primer Design Tool and ordered from Life Technologies. Below is the table of primers used in this project. The *DVL1* genomic sequencing primers were designed by Tim Morgan and Heleen Rösken, and the *CREB* and *DVL1*-Mutagenesis primers by Phil Daniel (all from the Robertson Laboratory).

Table 3.1. Sequences of primers.

DVL1-Restriction Fragment (forward)	5'-cccggaagtacgccagcagc-3'
DVL1-Restriction Fragment (reverse)	5'-ctggtaggcaggcgggaagc-3'
DVL1-Mutagenesis (forward)	5'-cacccggctgcccccggcctctgggtcag-3'
DVL1-Mutagenesis (reverse)	5'-ctgacccagaggccgggggcagccgggtg-3'
DVL1-cDNASeq 44 (forward)	5'-ttcgaattccgccatggcggagaccaag-3'
DVL1-cDNASeq 751 (forward)	5'-cctccttcagcagcataacc-3'
DVL1-cDNASeq 1517 (forward)	5'-gacttcggatcaggacacgc-3'
DVL1-cDNASeq 1793 (reverse)	5'-cgtgtgatccgattcactgc-3'
DVL1-cDNASeq 2067 (reverse)	5'-ccgggatccacgagtcacatgatgtcc-3'
DVL1-Exon14 (forward)	5'-caagatcaccttctccgagc-3'
DVL1-Exon14 (reverse)	5'-gcccaagtacacagcaggag-3'
DVL1-Exon15 (forward)	5'-ctcaagcatcggggtgag-3'
DVL1-Exon15 (reverse)	5'-gacacaggtgctgtcaggag-3'
CREB (forward)	5'-cagtatgcacagaccactgatgg-3'
CREB (reverse)	5'-tacgacactctcgagctgcttcc-3'

3.4.2. PCR

PCR was carried out using the KAPA Biosystems KAPA2G Robust kit (KK5004). 0.5 U of Taq DNA Polymerase, 300 µM of each dNTP, and 0.5 µM of the forward and reverse oligonucleotide primers, made to a final volume of 10µL with the 5x Kapa Mg^{2+}-containing buffer. Reactions were performed in a BioRad or MJ Research Dyad DNA engine. Unless otherwise stated programmes had an initial activation step of 94℃ for 2 min, followed by a variable number of cycles of 98℃ for 10 s denaturation, 60-72℃ annealing and then 72℃ extension. Programmes all finished with 2 min extension at 72℃.

3.4.3. Genomic and cDNA sequencing

In order to confirm the synthesis of plasmids or investigate the presence of the mutation genomic DNA, PCR, and plasmid were prepared for sequencing with the BigDye Terminator v3.1 Cycle Sequencing Kit (Applied Biosystems). 4 µL of PCR product or 550 ng of plasmid and genomic DNA were added to 1 U Illustra Shrimp Alkaline Phosphatase (GE Healthcare, E70092X) and 5U of Exonuclease I (New England Biolabs, M0293), and the solution made up to 14 µL with MiliQ water. This was incubated at 80°C for 20 min. 3 µL of this reaction was added to 5 nmol of primer, 1 µL of BigDye buffer and 1 µL of BigDye Enzyme mix and the solution made up to 10 µL with MilliQ water. The programme consisted of an initial denaturation step at 96°C for 1 min 15 s, followed by 24 cycles at 96°C for 45 s, 50°C for 45 s, and 60°C for 3 min 30 s (manufacturer's recommended conditions). After cycling 2 µL of 3M sodium acetate, 50 µL of 100% ethanol, and 10 µL of MilliQ were added and the reaction mixed, which was centrifuged for 20 min at 3000 rcf (Eppendorf 5415R) at room temperature. The supernatant was removed and pellet washed with 75 µL of 70% ethanol. The ethanol was then removed and the pellet left to air dry. The pellets were sent for analysis at Genetic Analysis Services at Otago University, who use an ABI 370xl DNA Analyser.

The *DVL1* reference transcript NM_004421.2 is used for the description of mutations within this thesis.

3.4.4. DNA gels

Electrophoretic DNA gels were used to visualise PCR products and cut plasmids. A 1.5-3% agarose gel was used appropriate to fragment size. 0.05% Ethidium

Bromide (Invitrogen) at 10 μL/40 mL gel or SYBR Green (Life Technologies S57567) used at 1/10,000 enabled visualisation with a UV FireReader (UVITEC Cambridge).

For purification the fragments were visualised using the prep setting on the UV-reader to identify the position of the desired band. Extraction was carried out with the QIAquick Gel extraction Kit (Qiagen 28704) following the manufacturer's protocol.

To quantify, the gels were visualised at sub-saturating exposures and either comparison to the DNA ladder or comparison directly between fragments was used to quantify either visually or using ImageJ.

3.4.5 Restriction enzyme digest of DVL1 PCR product

This was used to investigate the expression of the *mtDVL1* transcript. PCR product containing the mutation site from Case 1 was produced by amplification for 35 cycles with the DVL1- Restriction Fragment (forward and reverse, Table 3.1). 8μL of this product was then digested for 4 h at 60^{o}C with 1 μL of the restriction enzyme BstN1 (New England Biolabs, R0168) in the PCR buffer with the addition of 1μL of NEB3.1 buffer (from kit). A restriction enzyme negative control was treated in an identical manner, with the exception that the BstN1 was replaced with 1 μL of MilliQ water.

3.5. Synthesis of DVL1 expression constructs

3.5.1. Construction of mutant DVL1

The following process is also described in Figure 3.1. A wild-type clone of DVL1 in T7plus vector was available in the laboratory. Two mutagenic primer pairs: DVL1-cDNASeq 44 (forward) and DVL1-Mutagenesis (reverse); and DVL1-Mutagenesis (forward) and DVL1-cDNASeq 2067 (reverse), were used to generate 5' and 3' DVL1 fragments respectively (annealing temperature 65^{o}C, 20 cycles). The template plasmid was digested from the 3' reaction mixture using the restriction enzyme HindIII (New England Biolabs, R0104) in the 2.1 buffer (New England Biolabs) for 2 h, which left the 3' fragment intact. No suitable restriction enzyme was available for the 5' fragment so gel purification (as previously described) was used to separate the template plasmid from the PCR fragment. The two fragments were quantified by gel electrophoresis. 4 µL of each solution was then denatured at 95^{o}C for 2 min and then annealed for 5 min at 60^{o}C and 5 min at 72^{o}C. 4 µL of this reaction was then used as a template with the full-length DVL1 primers (DVL1-cDNASeq 44 (forward) and DVL1-cDNASeq 2067 (reverse)) annealing at 62^{o}C for 35 cycles. The product was gel purified (see Figure 3.1).

The mutated DVL1 was firstly polyA tailed and 5'-capped for expression, then cloned into the pcDNA 3.1 vector (Invitrogen, V795-20) with the TOPO®TA cloning kit according to the manufacture's instructions (Life Technologies 450641) in a 10 µL reaction. 50 µL of chemically competent *Escherichia coli* (*E. coli*) DH5α were transformed with 5 µL of reaction mix and immediately plated onto agar plates with ampicillin selection (100 µg/mL). This was incubated overnight at 37^{o}C and then the

colonies screened using a PCR reaction with the DVL1-cDNASeq 1373 (forward) and DVL1-cDNASeq 1634 (reverse) primers. Successful colonies were miniprepped, and Sanger sequencing used to confirm the fidelity of the transcript, then a maxiprep was used to generate large quantities of plasmid, quantified by nanodrop.

3.5.2. Attachment EGFP tags to DVL1 constructs

BamH1 and EcoR1 (New England Biolabs, R0136S and R0101S) in NEB buffer 2.1 for 1 h were used to cut the DVL1 from the pcDNA 3.1 Vector and open a pcDNA3.1 based EGFP-tagged (enhanced green fluorescent protein) plasmid (Addgene, 13031). The accepting plasmid was CIP (Alkaline Phosphatase, Calf Intestinal, New England BioLabs, M0290) treated to prevent re-annealing and the *DVL1* inserts gel purified from the untagged plasmid. Column purification with NucleoSpin Plasmid Kit (Macherey-Nagel 740588) following manufacturer's protocol was used to remove the restriction enzymes. Ligations were carried out overnight using a ~1:1 or 1:3 ratio of insert to cut vector, quantified by agrose gel (as previously described), with the T4 DNA ligase (New England Biolabs M0202).

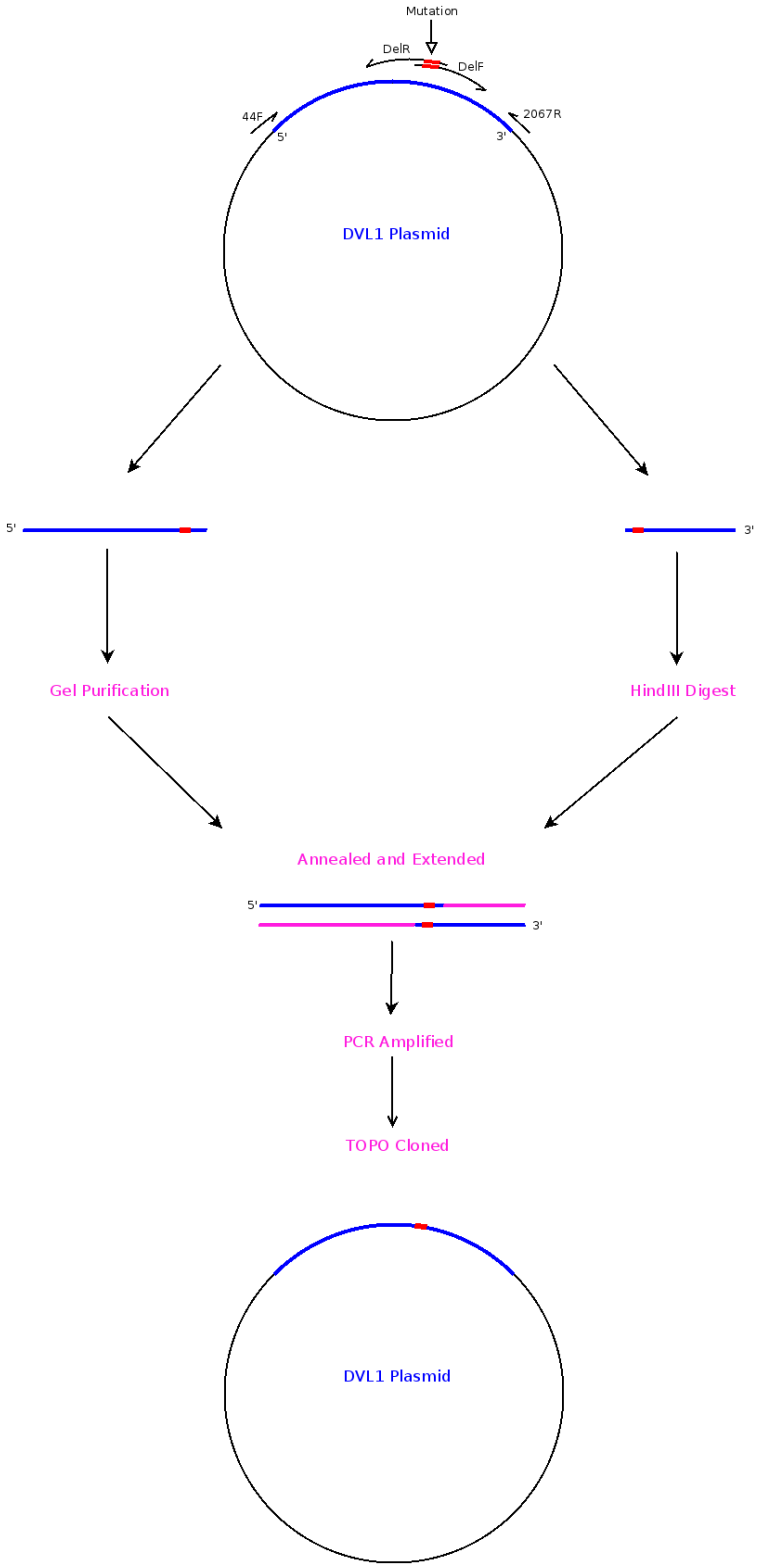

Figure 3.1. DVL1 mutagenesis protocol. This shows the various steps of the DVL1 mutagenesis as outlined in Section 3.5.1. The mutation is marked in red for clarity, the 'del' primers refer to the mutagenesis primers in Table 3.1.

3.5.3 Cloning of *DVL1* plasmids

5 µL of the ligation reaction was then combined with chemically competent DH5α *E. coli* in L.B media (10 g/L tryptone, 5 g/L yeast extract, and 10 g/L NaCl at pH-7.0) and immediately plated if ampicillin selection was used (for untagged constructs, 100 ng/mL ampicillin) or left for 1 h at 37°C if kanamycin selection was employed (for GFP-tagged constructs, 30-60 ng/mL kanamycin). These were incubated at 37°C over night. Colonies were then selected and screened by PCR using appropriate primers before the presence of the construct was confirmed by sequencing plasmid DNA (described below).

3.6. Production of DVL1 plasmids

3.6.1. Small Plasmid Preparations

Small DNA preparations were prepared from bacterial streaks grown overnight at 37°C. The Nucleospin Plasmid (Macherey-Nagel, 740588) kit was used to purify the plasmids after the bacteria were lysed in the lysis buffer (kit used according to the manufacturer's MiniPrep protocol).

3.6.2. Large Plasmid Preparations

Large DNA preparations were made from 80 mL cultures that were grown overnight at 37°C in a rotary incubator. The Nucleobond Xtra Midi Prep kit (Qiagen, 28106) was used according to the manufacturer's MidiPrep instructions.

3.7. DVL1 protein analysis

3.7.1. SDS-PAGE

SDS-PAGE (sodium dodecyly sulfate-polyacrylamide gel electrophoresis) was used to separate proteins before Western blotting to enable their identification and quantification. All gels were 8% Bis-acrylamide with 0.1% SDS and were run until the marker reached the end of the gel at 200 V. An SDS containing loading buffer (130mM Tris-Cl pH-8.0, 20% glycerol 4.6% SDS, 2% DTT, 0.02% bromophenol blue) combined with cell lysis buffer (Promega, E1531) was used to lyse the cells and 20 µL of these lysates were directly run on the gel or lysates were stored at -20^{o}C until needed. The running buffer consisted of 3 g/L Tris, 14.4 g/L glycine and 0.1% SDS.

3.7.2. Transfer from polyacrylamide to nitrocellulose

Transfers were carried out using the semidry TransBlot Turbo (Biorad), and transferred to 0.2µm nitrocellulose (BioRad, 162). Optimisation with ethanol and isopropanol supplementation of the transfer buffer (3 g/L Tris and 14.4 g/L glycine) was carried out, but it was concluded that the absence of alcohol led to the most reliable transfers. 9-10 layers of Whatman 3M filter paper were used in the transfer stack and the programme ran for 45 min at a maximum of 1.6 A or 25 V.

3.7.3. Antibody incubations

Membranes were blocked in 5% milk PBS at room temperature for 2 h. Incubations with all primary antibodies were conducted over night in 0.1% BSA in PBS-0.1% Tween at 4^{o}C. Anti-DVL1 (Rabbit, Abgent AP12326c), anti-GFP (Rabbit, Life Technologies A6455), and anti-GAPDH (Mouse, Sigma G8795) were used at 1:1,000, and anti-α-tubulin was at 1:250. The membranes were then washed for 3 x 10 min in PBS. HRP-

tagged secondary antibodies were applied for 1 h at 1:5000 in 0.1% BSA, PBS-Tween 0.1%. Alternatively IRDye® fluorescently tagged antibodies were applied for 1 h in 5% PBS-milk at 1:10,000. The membranes were then washed again as above. The SuperSignal West Pico kit (Thermo Scientific, 34077) was used for chemiluminescence and films were exposed for times of between 5 sec and 30 min as appropriate. The Odyssey CLx (LiCor) was used to visualise fluorescence.

3.8. Transient transfection assays

3.8.1. Transfections

To investigate the impact upon WNT signalling a number of luciferase-based transfection assays were carried out as described below. Either the wild-type *DVL1* (*wtDVL1*), the mutant *DVL1* (*mtDVL1*) or a truncated form of *DVL1* (*shDVL1*), which has a stop codon at the point of the mutation in Case 1 (i.e. it encodes a product similar to the mtDVL1, but does not have the new tail produced by the frameshift). All transfections were in C2C12 cells. These cells were split across 24-well plates, with 40,000 cells per well in 0.5 mL of modified DMEM. The cells were immediately transfected with 80 ng of TOPFlash Reporter plasmid and 20 ng of β-galactosidase as a normalising control. Variable amounts of *mtDVL1*, *shDVL1*, and *wtDVL1* vectors were transfected. Empty vector (pcDNA3.1 or) was used to ensure that the total DNA transfected (in ng) was consistent across an experiment. Cells were then incubated overnight before exposure to WNT3A containing media (available within the laboratory and produced from L-cells transfected with human WNT3A, a mouse enteric endocrine cell commonly used for this purpose, a technique first described in ref. 95) for 8 h, or simply incubated for 16-24 h. Subsequently the cells were lysed in 100 µL of firefly luciferase lysis buffer (Promega Kit, E1531).

3.8.2. Luciferase assays

The Promega Luciferase Assay System (E1500) was used. Cells were lysed at room temperature in 100 µL of the provided lysis buffer (made up to 1x with MilliQ water). 20 µL of the cell lysate per well was transferred to an opaque 96 well plate, which was kept on ice. The Synergy 2 Multi-Mode Reader (BioTek) pipetted 20 µL of luciferase reagent (from Promega Kit) per well and read the florescence for 3 s after a 1 s delay.

3.8.3. β-galactasidase measurement

After the luciferase reading the remaining lysis buffer was mixed 1:1 with a 2x β-galactosidase reagent prepared according to manufacturer's (Promega) instructions. This was incubated at 37°C until visible yellowing was present in all wells. An equal volume of 1 M Tris was added to stop the reaction and then 150 µL was pipetted to a transparent 96 well plate. The absorbance of this solution was read using Synergy 2 Multi-Mode Reader (BioTek) at a wavelength of 440 nm.

3.8.4. Normalising luciferase results

All luciferase assays were performed with an internal duplication, using two separate wells. The average of these two luciferase intensities was divided by the average absorbance (β-galactosidase) of the wells to give a luciferase value normalised to the transfection efficiency. In order to allow comparison across repeats, given the substantial absolute variation in luciferase activity, each normalised luciferase value was divided by the average luciferase value of the plate to produce a "relativised" value.

3.8.5. Statistics and graphs

All statistics were carried out using "R" (with the "R Studio" interface, http://www.r-project.org/). Data was log-transformed using the natural log to adjust for heterostochasticity when appropriate (in accordance with professional statistical

advice). One-way or two-way ANOVAs were used as appropriate, followed by post-hoc analysis using the Tukey Honest Significant Difference (HSD) test for the calculation of individual *P*-values. Graphs were drawn in Prism v6.0 (GraphPad).

4. CHAPTER FOUR –EXPRESSION OF ENDOGENOUS MUTANT DVL1

4.1. Strategy

Previous to this project a combination of whole-exome sequencing and direct Sanger sequencing identified mutations in two of the three patients studied here. A third patient, identified by phenotypic information available in the literature, was studied using direct Sanger sequencing (results detailed in this section).

We hypothesised that the similar mutations found in these three individuals were acting through a gain-of-function, which would require the expression of the mutant protein. Accordingly we investigated the presence of mRNA transcript in fibroblasts from Case 1, to exclude the nonsense mediated decay of the mutation-bearing transcript. Secondly we investigated the expression of mutant protein using Western blotting endogenous cell lysates from Case 1; the slight size differentiation between the mutant and wild type proteins predicted the presence of two bands.

4.2. Identification of mutations in Case 1 and 2

Before this work began a previous student in this laboratory, Heleen Rösken, used exome sequencing to identify the mutation in Case 1. At the time of this sequencing both Case 1 and 2 were known to the laboratory, and the absence of family history and consanguinity indicated that the phenotype was likely to be caused by *de novo* mutations. On this basis whole-exome sequencing using a parents-proband approach was taken to identify *de novo* variants in Case 1. Full methodological details of this approach is contained in the attached *American Journal of Human Genetics* paper, but two coding, rare, *de novo* variants in Case 1 were validated by Sanger sequencing, one in *DVL1* and the other in *TNRC6A*. The

DVL1 mutation is detailed shortly (Figure 4.2 and Table 4.1), but, in brief, it conferred a shift of the reading frame in the penultimate exon. *TNRC6A* encodes a component of the cytoplasmic ribonucleoprotein complex that regulates mRNA. The mutation in question (c.2753C>T, p.Pro918Leu, RefSeq NM_014494.2) was predicted by *PolyPhen* (a tool which predicts the deleterious nature of a variants on the basis of conservation and the physical properites of the amino acid changed) as likely to be benign.[96]

The same approach was taken in Case 2, but whole-exome sequencing identified no mutations in *DVL1* or *TNRC6A*. The sequencing coverage of the *DVL1* region was, however, low. On this basis Heleen Rösken and Tim Morgan (also from this laboratory) Sanger sequenced the *DVL1* exons of Case 2 and their parents (except for exon 1, for which functioning primers could not be designed). This revealed a very similar *de novo* mutation to Case 1, again producing a frameshift in the penultimate exon (Figure 4.2 and Table 4.1).

4.3. Genomic Sanger sequencing of Case 3

Our lab received samples from the Netherlands of Case 3 and her parents. We hypothesised that the mutation in this case was likely to be similar to those already identified in Cases 1 and 2. On this basis the penultimate and final exons of DVL1 were sequenced (Sanger chromatogram shown in Figure 4.1). A mutation was identified in the 3' half of the 14th exon, denoted as c.1576_1583delinsG, which, as in the previous cases, leads to a −1 shift in the reading frame, in this case p.Pro526Alafs*121 at the protein level (see Figure 4.2 for all three protein structures).

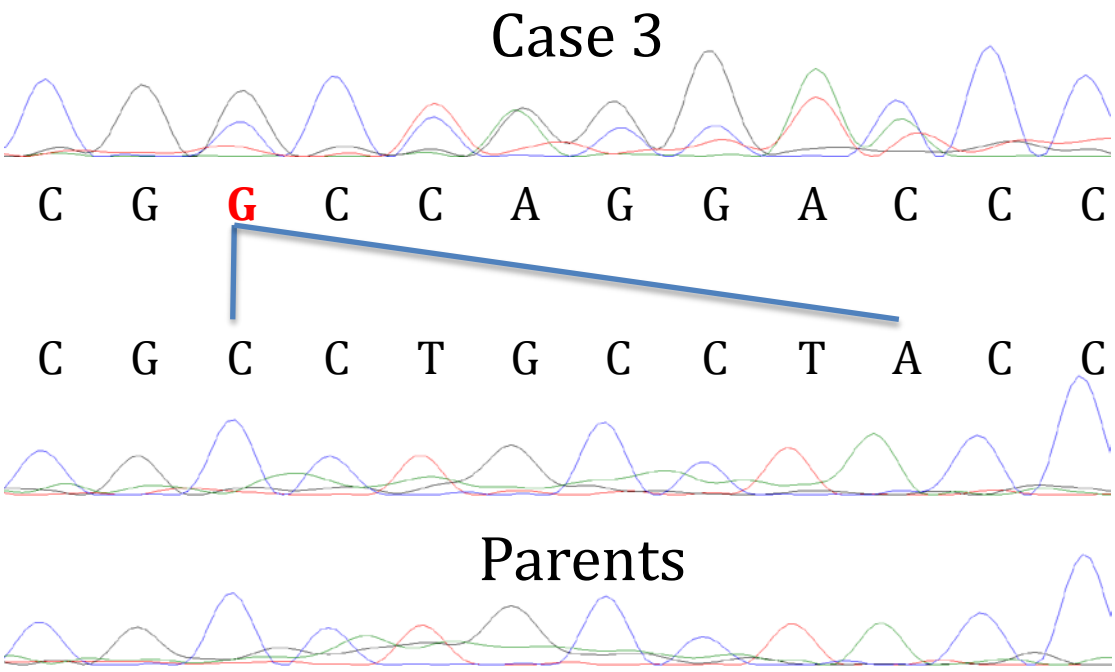

Figure 4.1. Sanger chromatogram from Case 3 and parents.
These are the results from the genomic sequencing of Case 3 (top) and parents (bottom). The mutation is an eight base deletion with a single base insertion (1576_1583delinsG) leading to a −1 shift in the reading frame (protein product: Pro526Alafs*121). The blue lines indicate the section that is deleted in the case but present in the parents, the red G is the inserted base. Note the presence of a 'double-trace' in Case 3 showing the presence of two transcripts present: the wild type and the frameshifted mutant – this indicates heterozygosity.

4.4. Summary of mutations in all three Cases

The mutations in all three individuals are in the 14th exon of *DVL1* and lead to a −1 reading frameshift. Each predicted mutant DVL1 protein is 23 residues shorter than wild type. All three have an identical 121-residue section of novel C-terminal sequence. The mutations differ by only 21 amino acids at the N-terminal aspect of the novel sequence (Table 4.1 and Figure 4.2). This new C-terminal sequence contains a large number of basic residues, raising the predicted pI of the C-terminal section of the entire protein from 9.5 to 12.5.[97]

Rare, similar, *de novo* mutations within the same region of *DVL1* in all identified unrelated cases of RS-OS provide compelling evidence that these *DVL1* mutations

are causative of RS-OS. The mutations may be exerting their effect through either a loss- or gain-of-function. On the basis of homozygous mouse knockouts of *Dvl1*[25] and the phenotype of individuals with chromosomal deletions of the *DVL1* containing region,[92] neither of which exhibit osteosclerosis or RS, we hypothesised that this mutation is acting through a gain-of-function rather than a loss-of-function. Driven by this hypothesis we investigated the presence of endogenous mutation-bearing mRNA transcript in cell lysates of Case 1.

Table 4.1. Mutations across the three cases.
Each mutation leads to the same reading frameshift and a novel C-terminal sequence. The last 121 C-terminal residues are identical across the Cases. The wtDVL1 length is included for comparison. Each mutant is 23 residues shorter than the wild type.

	cDNA	Protein	Length (AA)
wtDVL1	–	–	670
Case 1	c.1519del	p.Trp507Gly fs*142	647
Case 2	c.1562del	p.Pro521His fs*128	647
Case 3	c.1576_1583delinsG	p.Pro526Ala fs*121	647

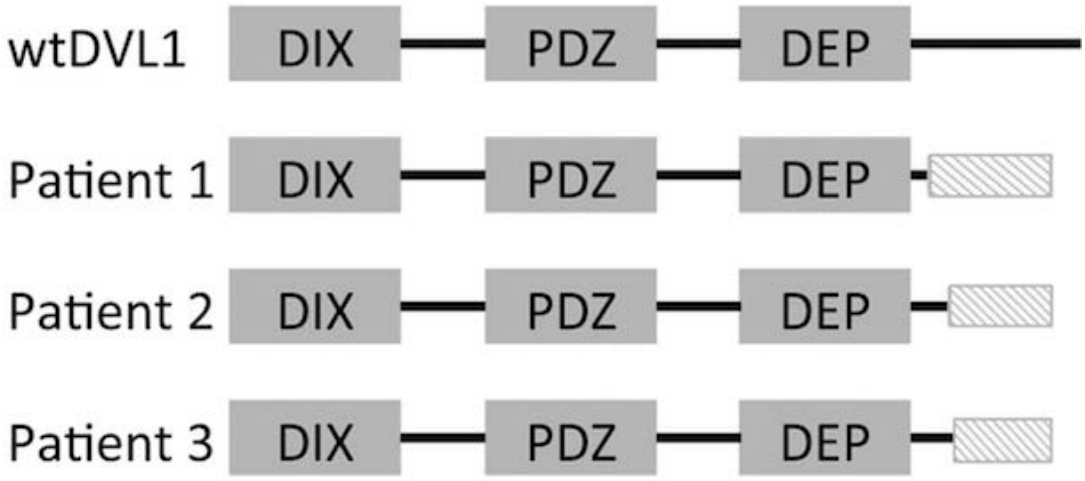

Figure 4.2. Cartoon of mutant and wtDVL1 proteins
The three main regions of DVL1 are shown as is the predicted novel C-terminal sequence caused by the frameshift mutations (shown by the shaded box). Note the substantial length of new C-terminal sequence present in the mutant proteins.

4.5. mRNA analysis

To investigate endogenous mRNA expression human fibroblasts extracted by dermal biopsy from Case 1 and an unrelated healthy control were cultured as described in Methods. RNA was extracted from a confluent 25mL flask and quantified by Nanodrop®-1000. cDNA was synthesised as described in Methods, and synthesis confirmed (contaminations was excluded with a reverse transcriptase negative control) with the reference *CREB* primers (see Appendix).

4.5.1. Sanger sequencing of mRNA transcript

Initially this cDNA was used for RT-PCR with the DVL1-cDNASeq 1477 (forward) and DVL1-cDANSeq 1793 (reverse) primers, this product was then sequenced. The sequenced trace revealed the presence of the frameshifted transcript in the mRNA population alongside the wild type DVL1 transcript (result not shown). This work is from my Summer Studentship, and it provides evidence that the mutant transcript persists and is not subject to nonsense mediated mRNA decay, which is consistent with the proposed gain-of-function of the mutant *DVL1* allele.

4.5.2. Restriction enzyme digest of mutant product.

To confirm the above result we used a restriction digest with an enzyme that would specifically recognise, and cleave, the wild type *DVL1* transcript while leaving the mutant intact. The DVL1-Restriction Fragment (forward) and DVL1-Restriciton Fragment (reverse) primers amplified the region containing the mutation from the Case 1 and a healthy control cDNA. This was digested by the restriction enzyme BstN1 (as the described in Methods), and the fragments separated by agarose gel electrophoresis. Figure 4.3 shows the results of the digest. The PCR product runs at the expected molecular weight (~180bp). In

molecular weight (~120bp, the other restriction fragment has a molecular weight too low to be seen on this gel). Some of the fragment is however refractory to digestion and remains at the original weight. In contrast the identically treated control digests to completion, leaving only a band at the digested molecular weight. It is worth noting that accurate quantification is not possible from this data due to the likely mutant-wild type heteroduplex DNA that will be represented within the of the PCR products (these heteroduplices would be resistant to restriction digest).

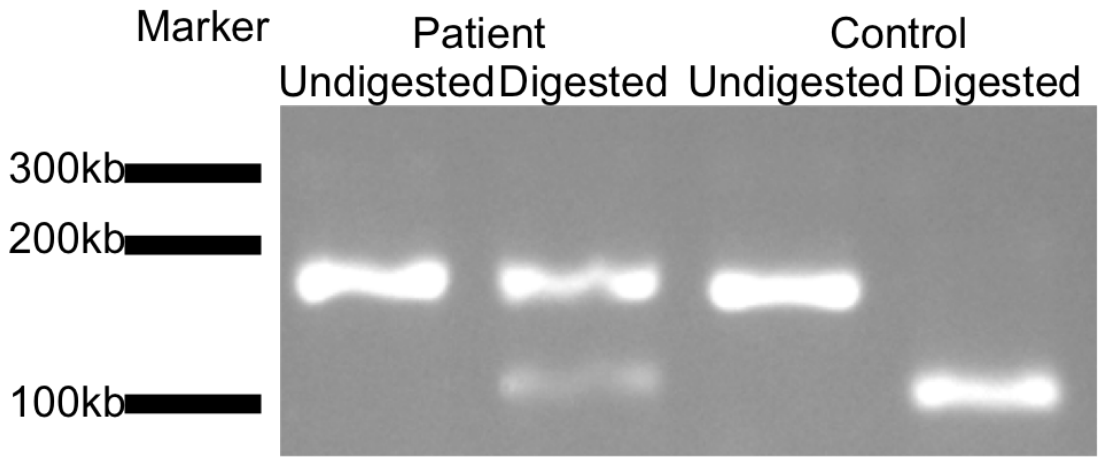

Figure 4.3. Restriction digest of Case 1 cDNA.
The undigested sample reveals a band of the expected molecular weight (~120bp) in Case 1 and in the healthy unrelated control. In Case 1 a fraction of the PCR product is refractory to digestion, whereas the digest proceeds to completion in the control, leaving only the band of the lower molecular weight (~60bp).

4.6. Protein analysis

Having confirmed the presence of mutation-bearing transcript we investigated the mutant DVL1 expression at the protein level. Using lysates from human fibroblasts from Case 1 and two controls endogenous protein expression was examined by Western blot with an anti-DVL1 antibody (Abgent, AP12326c) that has as its epitope the central portion of the protein (which is predicted to detect

both the mutant and wild type proteins). This revealed a band of the approximate molecular weight for DVL1, after SDS-PAGE using a small format gel, which was present in both the fibroblast cell lysates of the affected Case 1 and two unrelated and unaffected controls (not shown, work conducted during my Summer Studentship). Initial optimisation was carried out using the small format gel however this was found to be insufficient to separate mutant from wild-type protein by molecular weight (not shown). Mathematical modelling based on the migration of the molecular weight markers suggested that a large format gel would allow the resolution of the smaller mutant protein from the wild type. However this technique, despite providing the predicted separation (confirmed by the migration of the molecular weight marker), also failed to provide a separation of the two bands (Figure 4.4).

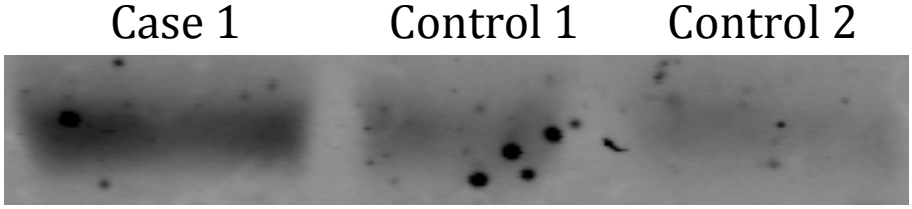

Figure 4.4. Western Blot of lysates with anti-DVL1 antibody.
Western blot of lysates from Case1 fibroblasts and two healthy, unrelated controls. Note the apparent, faint, single band present across all three samples, this ran at the approximate molecular weight of DVL1 (~73kDa). Visualised with chemiluminescence.

The isoelectric point calculator[98] was used to estimate the impact on the overall charge of DVL1 from the mutant C-terminus. The novel C-terminus was predicted to have a dramatic effect on the overall charge, raising the predicted pI of the entire protein from ~7 to ~10. This calculation does not take into account post-translational modifications which can have a substantial impact on charge (e.g. phosphorylation) but it provides an indication that there may be a

divergence in the pIs of the mutant and wild type DVL1 proteins. We hypothesised that this divergence in charge could be exploited to allow the separation of mutant from wild type protein in a native gel. On this basis a collaboration was undertaken with Dr. Alan Carne (University of Otago, Department of Biochemistry) who had the experience and resources to conduct 2D gel electrophoresis, which initially separates proteins in a native gel on the basis of charge and subsequently, in the second dimension, by molecular weight with SDS-PAGE. A number of unsuccessful attempts were made using this technique. Western blotting with the anti-DVL1 antibody, following 1D SDS-PAGE, produced a single band of the predicted molecular weight for DVL1 across all samples, as was previously found (Figure 4.4). However a sample of fresh culture media also showed the same band (Figure 4.5). This indicated that the commercial antibody was cross-reacting with a component of the media of the same approximate molecular weight as DVL1, rendering the detection of endogenous protein impossible with these components.

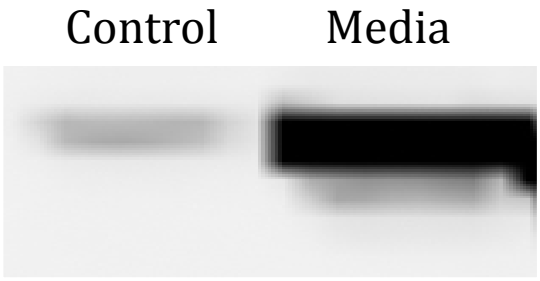

Figure 4.5. Western blot with anti-DVL1 antibody showing cross-reactivity.
The lysate from the control human fibroblast and fresh culture media both yielded a band running at the approximate molecular weight of DVL1. This indicates that the antibody is cross-reacting with a protein in the culture media of the same approximate weight of DVL1. This blot is visualised with chemiluminescence.

4.7. Summary of mutant DVL1 expression

All three Cases (including Case 3, who was identified in this project) show very similar *de novo* frameshift mutations, providing compelling evidence that these

DVL1 mutations are causative of RS-OS. The similarity between the mutations in the three cases supports the generalisation of experiments performed with endogenous cells from Case 1, or a construct bearing the mutation found in Case 1 (mtDVL1), to the other two cases (from which we do not have access to live cells). Supporting the proposed gain-of-function in Case 1 it was found that the mutant allele was expressed at the mRNA level through cDNA sequencing and a restriction enzyme digest. Detection of the protein from endogenous lysates proved impossible due to a cross-reactivity of the antibody to a component of the culture media. However the persistence of the mRNA transcript makes the presence of the mutant DVL1 protein plausible. The expression of mutant protein is investigated in the following section using a transfected tagged-DVL1 construct, which can be reliably detected by Western blot.

5. CHAPTER FIVE– DVL1 CONSTRUCT

SYNTHESIS AND EXPRESSION

5.1. Strategy

In order to study the effect of the RS-associated *DVL1* mutation expression constructs that could be transfected into WNT responsive cells (C2C12 cells) were required. Constructs were already available in the laboratory for the *wtDVL1* and the *shDVL1* (as described previously in Methods this is a truncated construct which terminates at the point of the mutation in Case 1, it is used to investigate the impact of the novel C-terminal sequence caused by the frameshift). However there was no construct available for the *mtDVL1*. Thus the first half of this section details the unexpectedly involved process of synthesising this mtDVL1 construct.

In order for the mutant *DVL1* to be acting through a gain-of-function the mutant protein must be expressed, and to assess this we required a detectable form of *DVL1*. The failure of the anti-DVL1 antibody (detailed in the previous chapter) meant that this detection necessitated the use of tagged constructs. Additionally the ability of DVL1 to form puncta (detailed in the Introduction, Discussion, and later in this chapter) is a requirement for canonical WNT signalling, which again has relevance to the proposed gain-of-function. A fluorescent tag would enable detection by Western blot and visualisation of the subcellular localisation of the mutant DVL1 by fluorescent microscopy. An EGFP-tag was chosen, as the laboratory possessed a robust anti-GFP antibody.

5.2. Direct cloning of mutant DVL1

Initially an attempt was made to clone the mtDVL1 directly from Case 1 cDNA. In order to facilitate the amplification of long sections of mRNA oligo-DT was used

as a primer in cDNA synthesis instead of random hexamers. The primers to the reference gene *CREB* (CREB-F and CREB-R) were used to confirm the cDNA synthesis (result not shown). A number of attempts were made to PCR the full length DVL1 using the DVL1-cDNASeq 44 (forward) and DVL1-cDNASeq 2067 (reverse) primers, however these all failed. Attempts were made to optimise the PCR using a temperature gradient, the Kapa GC-rich buffer, and supplementation with betaine (which aids PCR by reducing GC secondary structures), however none of these were successful, yielding gels without bands (results not shown). Direct cloning was abandoned at this point, and a mutagenesis approach was taken, as described below.

5.3. Mutagenesis of wtDVL1 plasmid

The steps of the mutagenesis are described in the methods section. After the purification of the 3' and 5' fragments quantification by gel electrophoresis showed an equivalent amount of both fragments (Figure 5.1) so a 1:1 ratio was used in the annealing. PCR amplification of full length was successful (Figure 5.1)

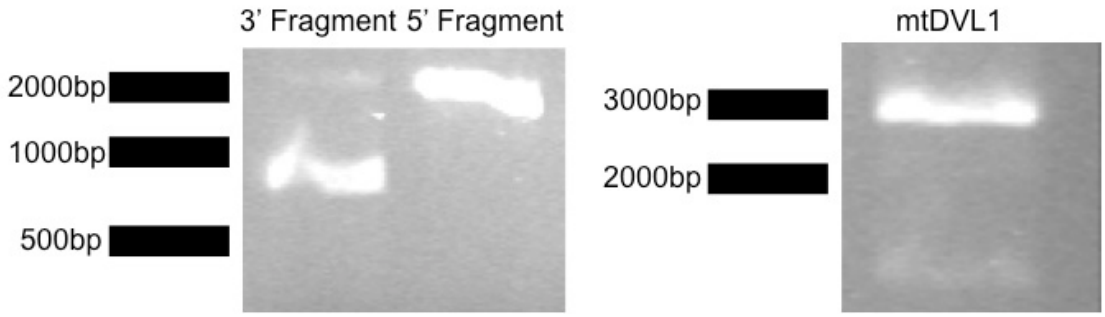

Figure 5.1. Intermediate results in the mutagenesis of the wtDVL1 plasmid.
The left hand gel shows the presence of the 3' and 5' fragments of the mtDVL1 running at the predicted molecular weights (produced with the mutagenesis primers from wtDVL1 plasmid), this gel was used to purify the fragments (as described in Methods). The right hand gel shows the successful PCR of the full length mtDVL1 from the annealed 3' and 5' fragments, this product was cloned.

The full-length *mtDVL1* (shown on a gel in Figure 5.1) was ligated into the pcDNA3.1 plasmid as described in Chapter 3.

The plasmid was cloned into chemically competent *E. coli* using the steps described in the methods section. 14 individual colonies were screened using the T7plus-F and the DVL1-2067R primers, which should selectively amplify only correctly orientated inserts. This PCR screen (in Figure 5.2) would allow the selection of colonies that were expressing the plasmid with the correctly oriented insert.

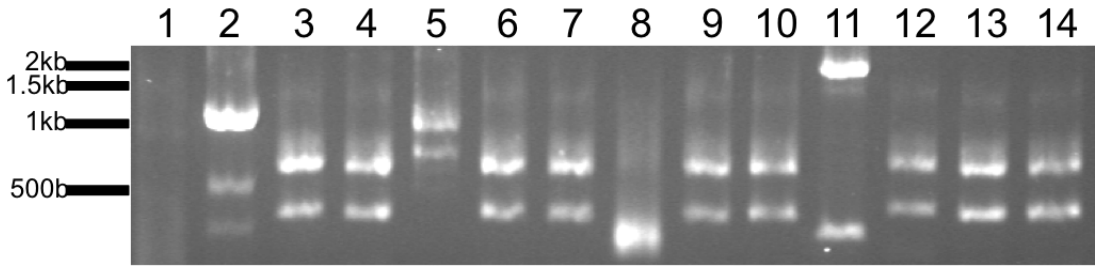

Figure 5.2. PCR screen of DH5α colonies.
The T7plus (forward) and DVL1-cDNASeq 2067 (reverse) primers were used to amplify the DNA extracted from the *E. coli* colonies. This pair of primers was predicted to only amplify plasmids with the correct orientation of the full-length *mtDVL1* vector. Only colony 11 from this screen revealed a band of the approximately correct molecular weight of *mtDVL1* (~2kb).

The PCR screen revealed that colony 11 was a likely candidate (see Figure 5.2), and on this basis a maxiprep was performed, and the insert sequenced. Sanger sequencing showed that despite the selective PCR screen the insert was not in the correct orientation, perhaps due to contamination of the sample. A second PCR screen of an additional 14 colonies (numbered 15-28) was performed as above, and colony 21 chosen on the same principles discussed previously (result not shown). A small plasmid preparation was made (see Methods) and sequenced, revealing that the insert was correctly oriented. A larger preparation

was performed and Sanger sequencing confirmed the presence of the insert in the correct orientation, and this construct was used in all future work.

5.4. EGFP-tag addition

The newly synthesised *mtDVL1* plasmids alongside the already available *wtDVL1* and *shDVL1* plasmids were used as a source of the *wtDVL1*, *mtDVL1*, and *shDVL1* inserts. Both the plasmids containing inserts and the empty EGFP plasmid were digested with EcoR1 and BamH1 as described in the Methods section, column purified, and then gel purified from the gel shown in Figure 5.3, as described in Chapter 3.

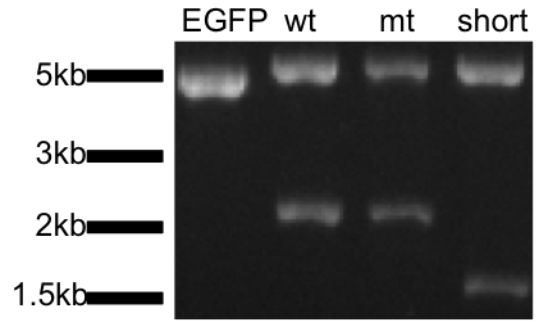

Figure 5.3. Restriction digestion of *DVL1* inserts cloned into the EGFP vector.
The right hand lane shows the open EGFP vector (note that it runs as a single band rather than a series of bands as you would predict from a circular plasmid). The three left hand bands show the removal of the *DVL1* inserts, note the substantially smaller length of the *shDVL1*, this is a truncated form of *DVL1*.

The EGFP and *DVL1* inserts were initially ligated for 2 h at room temperature with a 1:1 ratio of insert:vector as described in the Methods, but after a series of optimisations of the time and ratio was revised to an overnight digest with a 2:1 ratio of insert:vector. 5µL of this reaction mixture was incubated in 4mL non-selective LB media (described in Methods) with 100 µL of competent cells at 37^{o}C for periods ranging from 20 min - 2 h (30 min proved optimal) to allow the development of kanamycin resistance (the antibiotic resistance encoded in the

EGFP plasmid), before the cultures were spun down and spread on kanamycin selective plates (as described in Methods). These plates were incubated over night at 37^{o}C.

Given the difficulties in using the PCR screen to select for colonies expressing the plasmid (the false positive discussed previously) an alternative method was used. Four colonies were selected from each construct and miniprepped. A digest with BamH1 and EcoR1 was then used to screen for the presence of the insert (results not shown). Colonies that expressed the insert containing plasmid were then MaxiPrepped and Sanger Sequencing confirmed the presence of the correct insert (results not shown).

5.5. Expression pattern of EGFP-tagged constructs

As detailed in the Introduction and Discussion wild-type DVLs have a distinctive punctate expression pattern[33], and this pattern of expression is important to DVL function[34] (see Discussion). The region of DVL responsible for this pattern, as stated previously (Introduction) is the DIX domain,[37] which falls outside the region affected by the mutation. We therefore hypothesised that the mtDVL1 would show a similar punctate expression pattern. To investigate this, EGFP-tagged constructs were transfected into C2C12 cells at both 50 ng/well and 100 ng/well and the cells viewed after 20 h. It was determined that the best images were found at 100 ng/well, Figure 5.4 shows representative results of three full technical repeats.

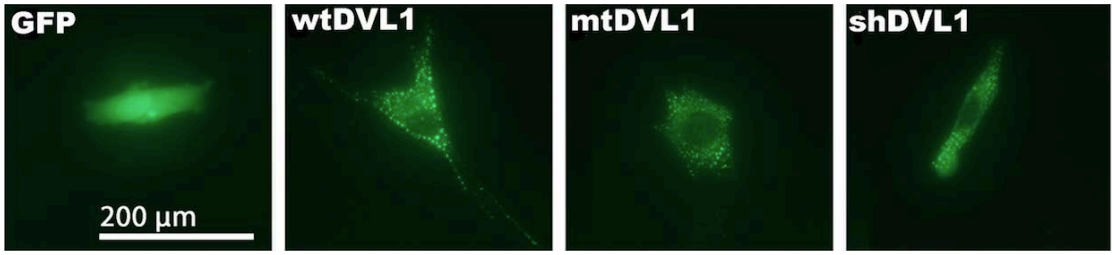

Figure 5.4. Fluorescent images of the EGFP-tagged DVL1 constructs.
Note the similar punctate expression pattern between each EGFP-DVL1, which contrasts with the expression pattern of EGFP (included as a reference).

All three constructs show a punctate expression pattern, with an apparently cytoplasmic distribution, which differs from the expression pattern of GFP (Figure 5.4). No apparent striking differences in subcellular distribution were noted between cells transfected with any of the *DVL1* constructs.

5.6. Western blot

The level of protein expression of each construct is clearly an important question, especially given the inability to detect endogenous mutant DVL1 (see Chapter 3). As previously discussed we hypothesised that this mutation was acting through a gain-of-function, which also led us to hypothesis that the mutant protein was produced and stable, which was visually supported by the EGFP fluorescence detailed above. In order to assess the relative expression of each transfected *DVL1* construct Western blotting was deployed after SDS-PAGE, as described in the Methods section. It was found that a single well yielded an insufficient amount of protein to detect (both with the anti-GFP antibody and anti-GAPDH). Thus four wells were combined in a total volume of 100 µL of SDS-lysis buffer (as described in Methods). The blot was visualised by chemiluminescence. All three *DVL1s* expressed at relatively similar levels (more quantitation follows) compared to a GAPDH control (Figure 5.5).

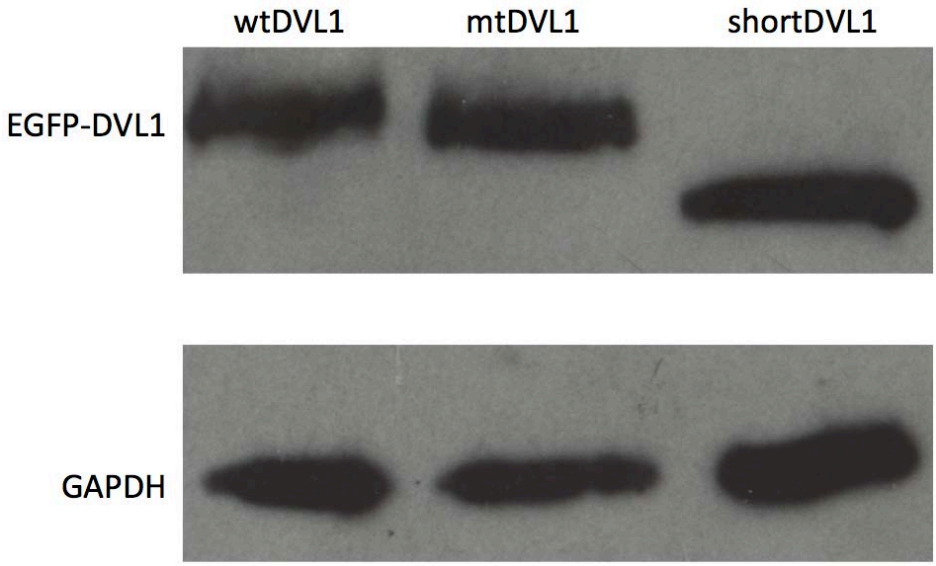

Figure 5.5. Western Blot of transfected GFP-tagged DVL1 constructs.
Note the slight difference in molecular weight between the wtDVL1 and shDVL1 (a difference of 21 amino acids, referred to as shortDVL1 on this figure) and the striking difference between the shDVL1 and the other two constructs. GAPDH is used as a loading control. This blot was visualised with chemiluminescence.

5.7. Quantitative Western blot

To quantify the protein level three repeat transfections (same method as previous section) were carried out and visualised using the Odyssey fluorescent detection system (LiCor) and appropriate antibodies. It was found that the previous control of GAPDH was not reliably detected on this system so an alternative control of α-tubulin was deployed. The Western blot is shown in Figure 5.6. The relative expression of each construct, normalised to α-tubulin, is as follows: *wtDVL1* 1.0±0.2 (SEM), *mtDVL1* 1.6±0.3, and *shDVL1* 2.0±0.2 (see Figure 5.6). A significant difference was found between the expression of the *wtDVL1* and *shDVL1* by one-way ANOVA followed by Tukey HSD tests ($P < 0.05$). No other significant differences were identified. Note the lower molecular weight protein in the *mtDVL1* expression, this is considered in the Discussion but its exclusion from quantification did not significantly change the relative expression (*mtDVL1* expression would be 1.2±0.2 if the second band is excluded).

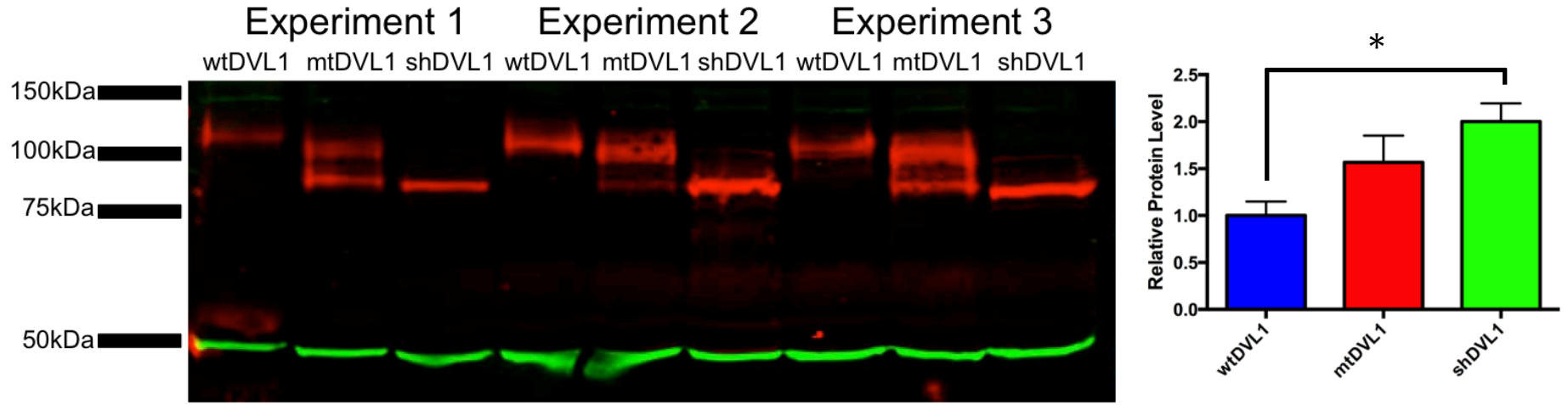

Figure 5.6. Quantitative Western blot of DVL1 constructs.
On the left is the Western blot that shows the relative protein level of the EGFP-tagged DVL1 constructs (~100kDa, red) across three independently performed transfections. The α-Tubulin is included as a loading control (~50kDa, green). On the right is a graphical representation of the relative protein levels (normalised to α-tubulin). The wtDVL1 level was 1.0±0.2 (SEM, indicated by error bars), the mtDVL1 was 1.6±0.3, and the shDVL1 was 2.0±0.2. One-way ANOVA followed by Tukey HSD tests revealed a significant difference ($P < 0.05$) between the wtDVL1 and shDVL1 only (marked with * on the figure). Note the smaller molecular weight product in the mtDVL1 lane particularly obvious in experiments 1 and 3. This has been visualized in *wtDVL1* expression on other Western blots (data not shown). For the quantitative analysis above the smaller product was included, if it is excluded no additional significant differences are revealed (the *mtDVL1* then expresses at 1.2±0.2).

5.8. Summary of transfected DVL1 expression

The mutagenesis of the wild type *DVL1* to produce a *mtDVL1* (which corresponds to the mutation found in Case 1) was the first necessary step for the subsequent investigations. The addition of the EGFP-tags to each of the constructs enabled the investigation of both the subcellular distribution and protein expression. The similarity in subcellular distribution indicates that DVL1, in the absence of C-terminal and in the presence of mutant C-terminal, will still form the supramolecular puncta in an apparently similar distribution to wild type DVL1. The quantitative Western blot data shows that there is no significant difference in protein level between the *wtDVL1* and *mtDVL1* expression but the amount of *shDVL1* protein is significantly increased. Possible reasons for this increase are considered in the Discussion. Critically, however, the quantitative information indicates that the mtDVL1 is not degraded to a greater degree than the wtDVL1 in these assays (if anything it may be more stable, even if the second product was removed from the calculations). This supports the hypothesis that the mutant transcript, which was present in the affected individuals (as shown in Chapter 4), is translated into a stable protein, which is likely to persist within the cells of the affected individuals. The next chapter addresses the biochemical impact of this mutant DVL1 protein on the canonical WNT signalling pathway.

6. CHAPTER SIX – DVL1'S IMPACT ON CANONICAL WNT SIGNALLING

6.1. Strategy

As outlined in the Introduction it is the osteosclerotic aspect of the clinical phenotype that is of particular interest to this work. Osteosclerosis is a rare clinical finding, and the pattern of generalised osteosclerosis in these individuals is reminiscent of the *LRP5*[51] and *SOST*[44] mutations (detailed in the Introduction). Both of these cause an over-activity in the canonical WNT pathway, which leads to an osteosclerotic phenotype.[4,51] Given the identification of mutations in a WNT mediator, *DVL1*, as causative of RS-OS and the similarity to the bone phenotype seen in over-active WNT signalling it seems likely that these mutations are acting to increase canonical WNT signalling.

This chapter aims to address the impact of *mtDVL1* on canonical WNT signalling. We hypothesise that mtDVL1 will be more active in the canonical WNT pathway than wtDVL1. The TOPFlash-based transient transfection assays detailed in this chapter aim to investigate this hypothesis. Secondarily, by comparison to the truncated DVL1 (shDVL1), this chapter also investigates the functional impact of the novel C-terminal sequence caused by the frameshift mutations in the affected individuals. Given the presence of the identical, novel, C-terminal sequence (see Chapter 3) in all three individuals we hypothesise that the new C-terminal sequence has an impact on the function of the mtDVL1, which is distinct from the truncation of the wild type C-terminal sequence alone.

The TOPFlash reporter assay is a well-validated readout of the canonical WNT signalling pathway. This reporter contains three T-Cell Factor (TCF) response elements, which, in response to canonical WNT stimulus drive the expression of

a firefly luciferase.[99] The TOPFlash reporter is deployed in this section to measure canonical WNT activity. As well as the TOPFlash a PDX11 plasmid, which constitutively expresses a β-galactosidase enzyme, is also used. The β-galactosidase causes a colour change in a β-galactosidase substrate, which is proportionate to the amount of enzyme. This second readout is used to adjust for differences in transfection efficiency between wells. The luciferase reading is divided by the β-galactosidase activity reading to generate a "normalised" result. Each normalised readout from a plate is the "relativized" by dividing by the average of the entire plate. Repeats can then be compared using this relativized reading, which adjusts for the substantial difference in absolute luciferase activity across identical repeats. As a whole this assay system acts as a robust readout of canonical WNT signalling in WNT responsive cells, such as the mouse C2C12 cells used in this chapter.

6.2. Impact of the expression of DVL1 constructs on canonical WNT signalling

Primarily we hypothesised that the mtDVL1 would be more active in the canonical WNT pathway than the wtDVL1, and, as a secondary comparison, that the mtDVL1 would behave differently to the shDVL1. To investigate the pattern of activity of all three *DVL1* construct increasing levels of DNA levels, from 0.5 ng/well to 32 ng/well, were transfected and the cells incubated for 18 hours. The cells were then lysed and the luciferase activity read. Results are reported as a fold increase over empty vector. The wtDVL1 construct caused an approximately linear increase in canonical WNT signalling with the addition of more plasmid, up to ~29-fold over that of the empty vector at maximum amount of DVL1 used

in the transfection (32 ng/well). The shDVL1 showed a similar pattern of activation but only reached a maximum of ~19-fold over the empty vector. Intriguingly the mtDVL1 showed a completely different pattern, raising the luciferase activity over that of the empty vector (~3.5-fold by 8 ng/well) but then showing no further increase with increasing levels of transfection. The results of three separate experiments are present in Figure 6.1. Error bars are standard error of the mean. Log transformed 2-Way ANOVA revealed a significant difference between the mtDVL1 activity and each other construct ($P < 0.00001$). The difference between the wtDVL1 and the shDVL1 was not significant at ($P > 0.5$). Post-hoc Tukey HSD tests found a significant difference between the mtDVL1 and each other construct at 16 and 32ng/well.

This result is inconsistent with our primary hypothesis: in this assay the mtDVL1 was significantly less active in the canonical WNT signalling pathway than the wtDVL1. The mtDVL1 and shDVL1 did, however, behave in a different manner. This supports the hypothesised additional function of the novel C-terminal sequence – yet, as with the comparison to wtDVL1, the novel function observed in this assay is not an increased activation of canonical WNT signalling.

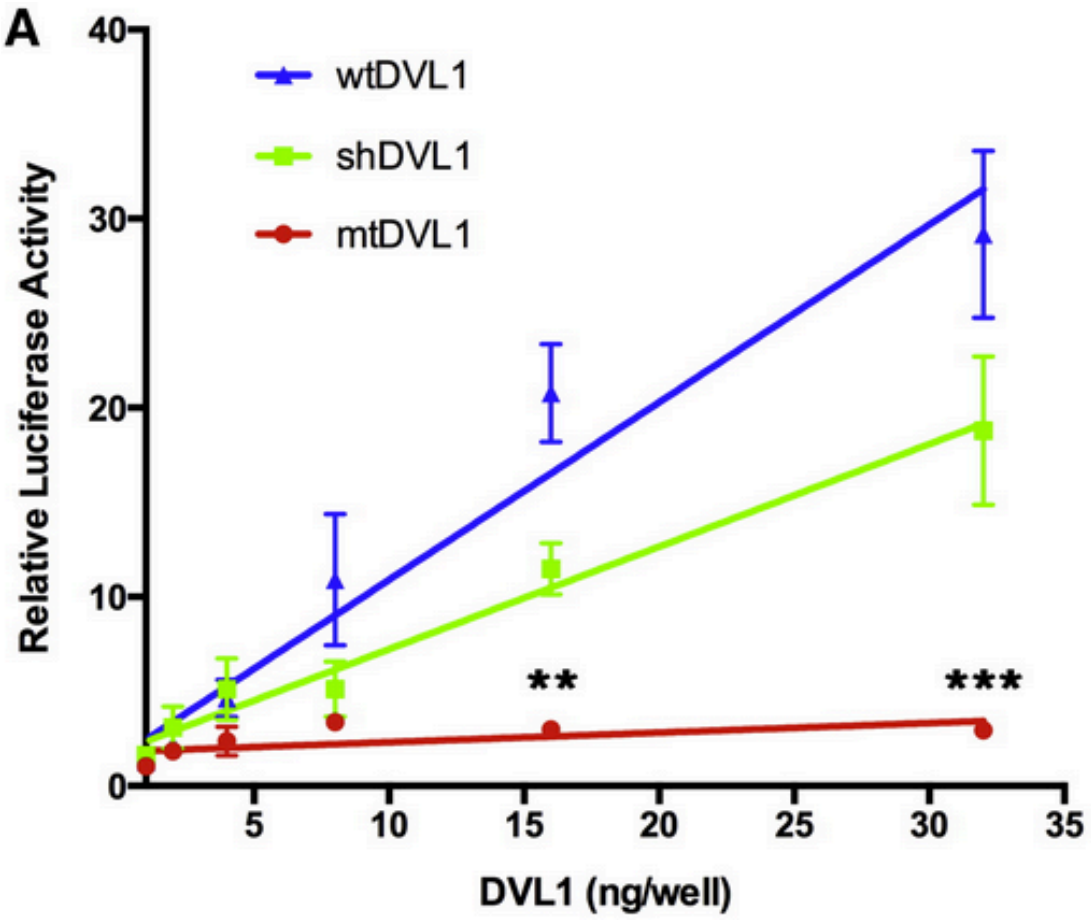

Figure 6.1. Luciferase activity with increasing DVL1 transfection.
Each DVL1 construct was transfected at 0.5 ng – 32 ng/well. The luciferase activity is reported as a fold increase over an empty vector control. Note the similarity between the wtDVL1 and shDVL1 activity (approximately linear increase in luciferase activity), and in contrast the failure of the mtDVL1, after an initial increase, to further increase luciferase activity. A log transformed 2-way ANOVA found a significant difference (P< 0.00001) between the mtDVL1 and the other two DVL1 constructs. Post-hoc Tukey HSD test found significant differences at 16 and 32 ng/well between the mtDVL1 and the other DVL1 constructs ($P < 0.01$ = ** and $P < 0.001$ = *).**

6.3. DVL1 constructs' sensitivity to WNT stimulus

In the previous experiment no additional WNT ligand was added to the media, and we hypothesised that the mtDVL1 may be more sensitive than wtDVL1 to WNT stimulus. To investigate this WNT3A (a well-established canonical WNT ligand) stimulus using L-cell conditioned media (see Methods) was assessed. The canonical activity of each *DVL1* at a high level of expression is unlikely to be

modelling an endogenous phenomenon, so the lowest level of expression where each *DVL1* had a notable effect upon WNT signalling was chosen to investigate the response to WNT3A (4 ng/well – effect was judged from Figure 6.1). The C2C12 cells were transfected with the appropriate *DVL1* construct then incubated overnight. WNT3A conditioned media was added at 5-15% (control L-cell media was used to keep the volume constant across the wells), and the cells were incubated for 8 h. As seen in Figure 6.2 all cells respond to the increasing percentage of WNT3A conditioned media with increasing luciferase activity (including the empty vector control). Disproving the hypothesis of an increased sensitivity of the mtDVL1 to WNT ligand no significant differences were found between the DVL1 constructs in a 2-way ANOVA, with Tukey HSD post-hoc analysis. It is notable that, in contrast to the high level of expression, at this lower level of transfection the mtDVL1 has a similar effect on luciferase activity to the other DVL1 constructs.

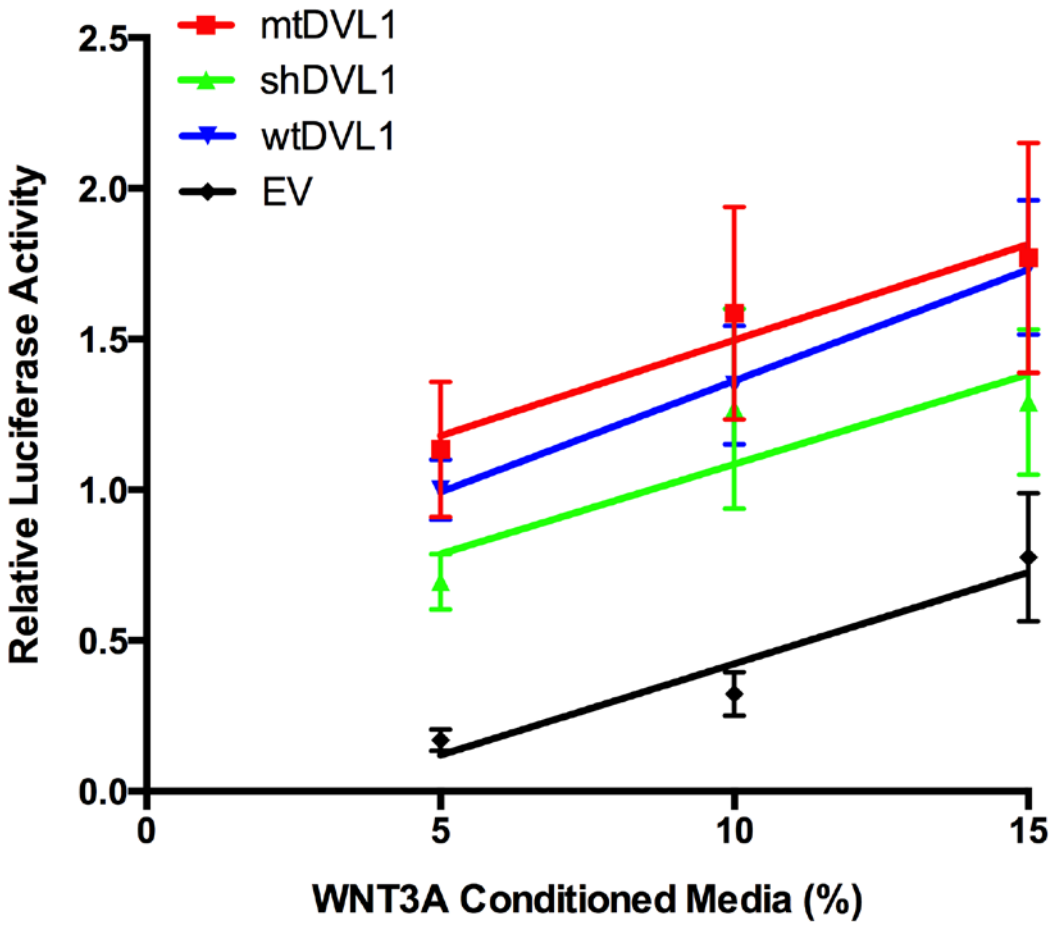

Figure 6.2. DVL1 constructs' impact on the C2C12 response to WNT3A.
Results are reported as fold over wtDVL1 activity at 5% WNT3A conditioned media stimulus. These are the results from 4 independent experiments, error bars are SEM. An empty vector transfection is included as a control to demonstrate the C2C12 endogenous response to WNT3A stimulus. The differences visible between the DVL1 constructs were statistically insignificant (two-way ANOVA, Tukey HSD tests).

6.4. Synergy between co-expressed mtDVL1 and wtDVL1

Given that the affected individuals are heterozygous and the earlier work in fibroblasts from Case 1 indicated the presence of both mutant and wild type transcript (Figure 4.3) we hypothesised that the abberant function of the mtDVL1 may depend upon the presence of wtDVL1. To investigate this *mtDVL1* was co-expressed with *wtDVL1* (the *shDVL1* was again included to determine the

relevance of the novel C-terminal sequence found in the mutant but absent in the truncated form). The same, low, fixed amount of *DVL1* construct was used as in the previous section (4 ng/well), however there was no additional WNT stimulus. Each *DVL1* construct expressed alone was compared to a 1:1 ratio of *wtDVL1* to *mtDVL1* or *shDVL1* (at the same total amount of *DVL1* per well, e.g. 2 ng of wtDVL1 and 2 ng of mtDVL1/well). C2C12 cells were transfected and incubated with the appropriate constructs for 24 h. Each DVL1 caused a comparable increase in WNT activity over the empty vector, similar to the effect observed in the presence of WNT ligand (Figure 6.2). The co-expression of *sh/wtDVL1* at the same total amount of *DVL1* caused a non-significant ($P > 0.1$) ~1.6-fold rise in luciferase activity over that of the wtDVL1 alone. The *mt/wtDVL1* co-expression led to an ~3-fold increase in the canonical WNT activity over the wtDVL1 alone, this was significantly different from each other construct ($P < 0.01$). The results of 5 independent experiments are displayed in full in Figure 6.3, relative luciferase activity is a fold of wtDVL1, error bars are the standard error of the mean, statistical analysis was with a one-way ANOVA followed by Tukey HSD post-hoc tests.

This result supports the initial hypothesis of this chapter that the mtDVL1 activated canonical WNT signalling. However this action requires the presence of wtDVL1. Additionally the significant difference between the *mt/wtDVL1* and *sh/wtDVL1* co-expressions supports the proposed additional function of the novel C-terminal sequence.

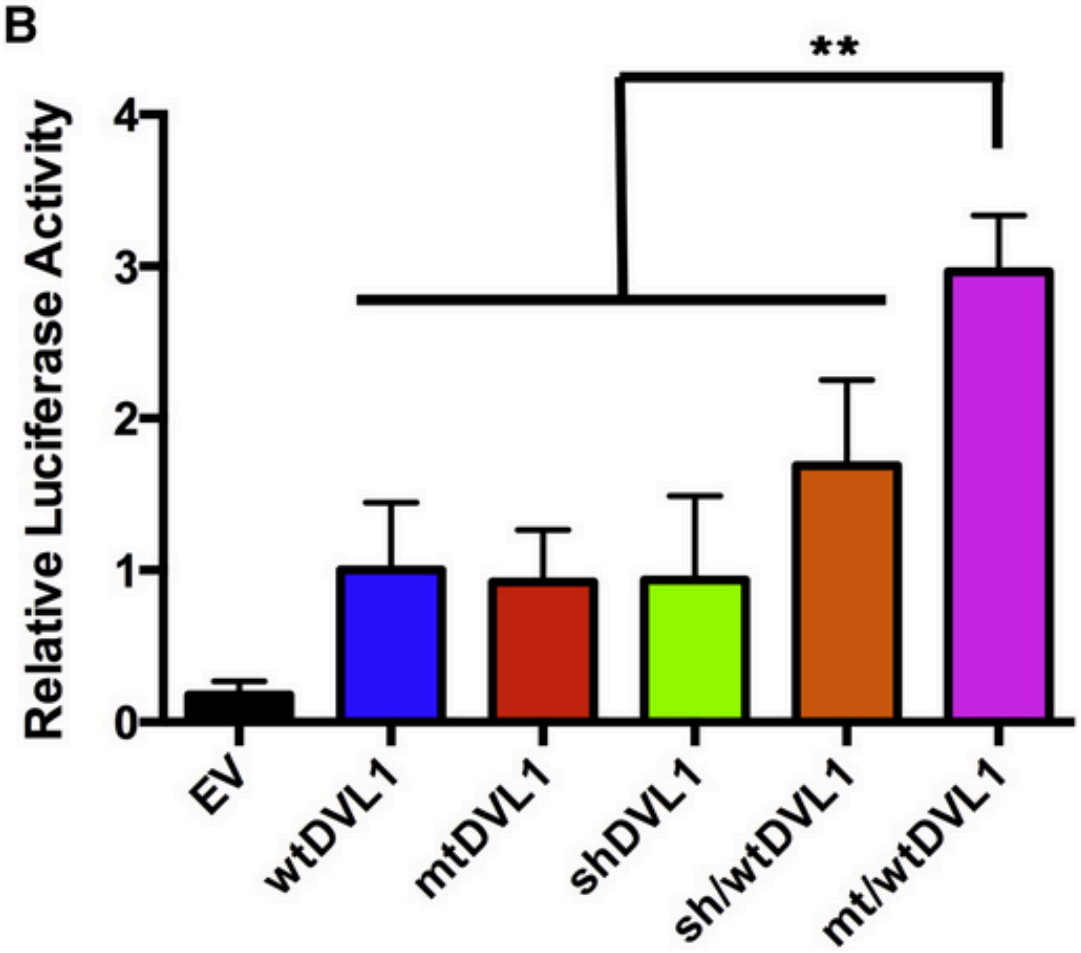

Figure 6.3. Synergy between mtDVL1 and wtDVL1.
Each well was transfected with 4ng of construct (either an empty vector control, a single DVL1 construct, or a 1:1 ratio of mt or sh to wtDVL1) and luciferase activity was measured after a 24 h incubation. Results are presented as a fold over the wtDVL1. Error bars are SEM. A significant difference in a one-way ANOVA followed by Tukey HSD post-hoc tests was found between the mt/wtDVL1 co-expression and each other DVL1-transfected cells ($P < 0.01$, indicated by **). No other significant differences were found between the DVL1 constructs, although the sh/wtDVL1 caused an ~1.6-fold increase over that of the wtDVL1 this was not significant ($P > 0.1$).

6.5. DVL1 co-expression and sensitivity to WNT stimulus

Finally, to further investigate this 'synergy', the response to WNT stimulus of the co-expressed *DVL1* constructs (i.e. *mt/wtDVL1* and *sh/wtDVL1*) was assessed. The method of WNT stimulus previously described was followed, using L-cell derived WNT3A conditioned media. The difference between the *mt/wtDVL1* and the *sh/wtDVL1* co-expressions was maintained, as was the increase in luciferase activity over *wtDVL1* expression in the *mt/wtDVL1* co-expression (Figure 6.4). Both co-expressed *DVL1* conditions responded with a comparable linear increase with an increased amount of WNT3A conditioned media, which was similar to the pattern observed in the individual DVL1 constructs (Figure 6.2, the empty vector and wtDVL1 response from this figure have been included in Figure 6.4 for comparison). A two-way ANOVA found a significant difference between the *mt/wtDVL1* co-expression and each other condition ($P < 0.01$). The *sh/wtDVL1* construct did not, as observed without WNT stimulus (Figure 6.3), increase the luciferase activity significantly over that of wtDVL1 alone.

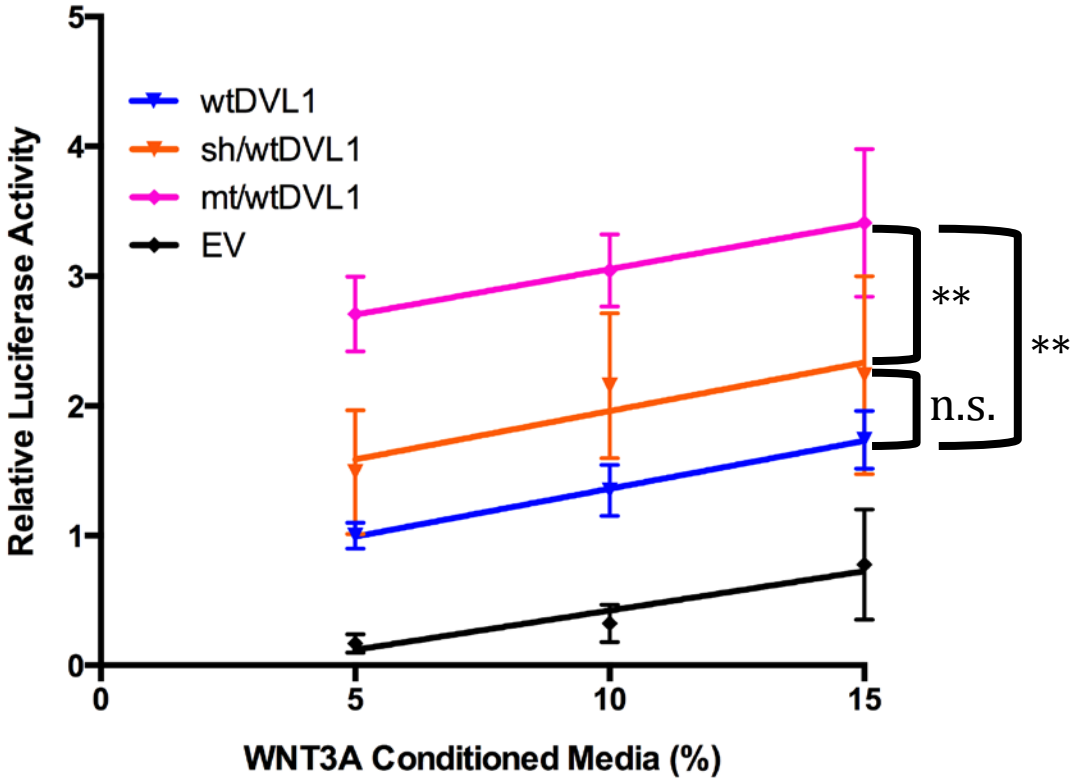

Figure 6.4. The co-expressed DVL1s and response to WNT stimulus.
At a fixed amount of mt/wtDVL1, sh/wtDVL1, and wtDVL1 (4 ng/well) increasing amounts of WNT3A conditioned media was used to stimulate the C2C12 cells (5-15%). Results are displayed as a fold of wtDVL1 at 5%, with error bars as SEM. The significant increase (*P* < 0.01 = **) in luciferase activity observed in mt/wtDVL1 over that of wtDVL1 and sh/wtDVL1 without WNT (Figure 6.3) expression was maintained. The pattern or response to WNT3A remained the same across all of the DVL1 conditions (but only wtDVL1 is shown here for clarity).

6.6. DVL1 impacts canonical WNT signalling independent of stimulus with WNT ligand

An incidental finding in this research is that WNT3A stimulus appears to affect WNT signalling in a manner that is independent of *DVL1* transfection (i.e. the canonical WNT stimulatory effects of WNT3A and DVL1 are mathematically independent of each other in these assays). Figure 6.5 shows the same data as in Figure 6.4 with the empty vector control (the empty vector is shown in Figure 6.2 and Figure 6.4) subtracted from each of the transfections' luciferase activity. This flattens the relationship (see Figure 6.5) between WNT3A stimulus and increasing luciferase activity. There is an initial increase in luciferase activity with the addition of exogenous *DVL1* (across all *DVL1* constructs) this increase does not, however, potentiate the response to WNT3A stimulus (the relationship between *DVL1* transfection and WNT3A stimulus on canonical WNT signalling is additive not multiplicative). This statistical independence of the two variables (WNT3A stimulus and *DVL1* transfection) would be consistent with some interesting biochemistry, which will be considered in the Discussion.

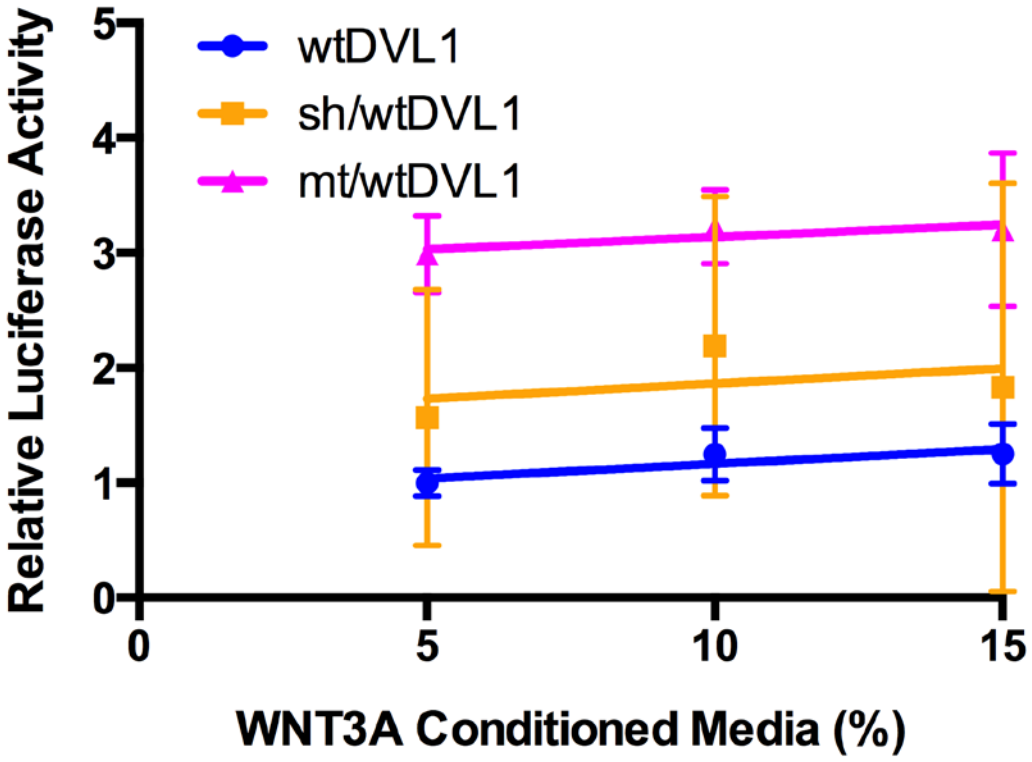

Figure 6.5. Effect of DVL1 on endogenous C2C12 WNT3A response.
Results are expressed as fold of wtDVL1 at 5% and error bars are SEM. This data is the same as that shown in Figure 6.2 and Figure 6.4, however the empty vector result has been subtracted from each condition. This transformation flattens the relationship between luciferase activity and WNT3A stimulus, this indicates that the rise in luciferase activity with increasing WNT stimulus is due to the endogenous C2C12 response to WNT3A, and is not dependent upon the transfected exogenous DVL1.

6.7. EGFP-tags do not disrupt DVL1 signalling

In sections 5.5, 5.6, and 5.7 EGFP-tagged constructs were used to confirm the expression pattern and level of *mtDVL1* and *wtDVL1*. This experiment confirms that there was no substantial alteration in WNT signalling function of DVL1 from the addition of the EGFP-tag. Figure 6.6 shows the results of three independent luciferase assays with the EGFP-tagged constructs at 100 ng/well (the amount used in sections 5.5, 5.6, and 5.7). There was no significant difference (one-way ANOVA, Tukey HSD tests, $P > 0.5$) between the EGFP tagged or untagged

constructs with either the mtDVL1 or wtDVL1. The EGFP-tags caused no increase in the WNT stimulatory ability of the mtDVL1, and caused only a slight, non-significant, decrease in the WNT activation from the wtDVL1. This supports the validity of using the EGFP-tag to investigate the expression pattern and level of the *DVL1* constructs, as it does not appear to dramatically effect function.

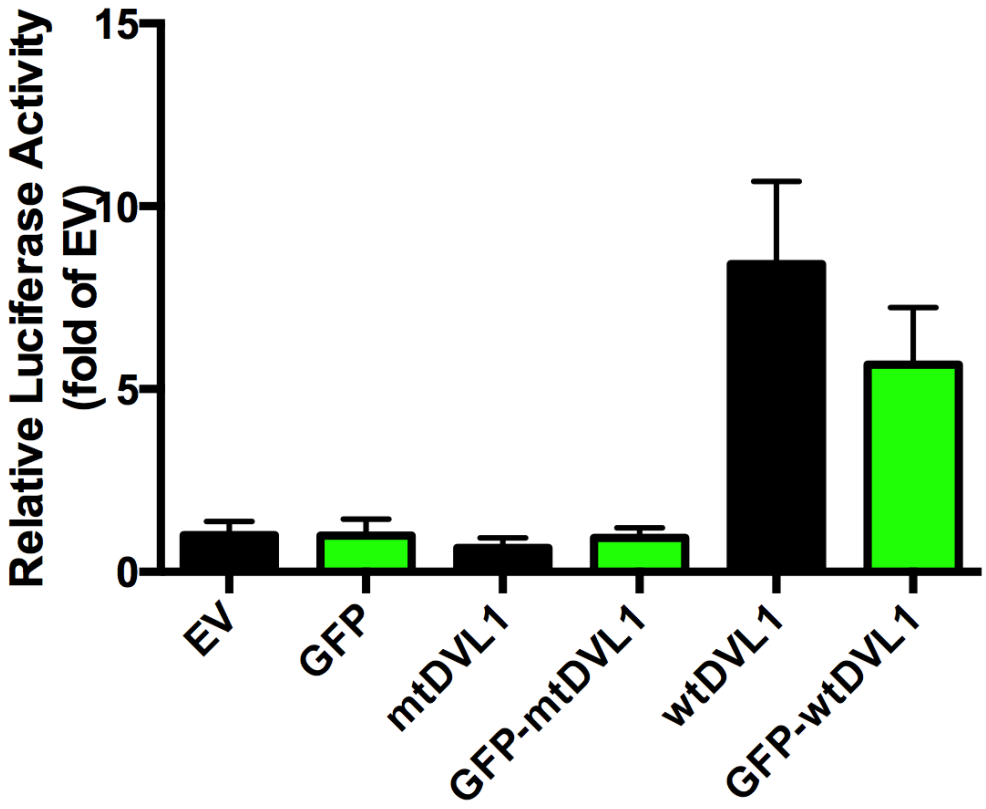

Figure 6.6. Impact of EGFP-tags on canonical WNT signalling.
This shows the results of three independent experiments at 100 ng/well of EGFP-tagged (denoted as "GFP") and untagged mutant and wild type DVL1 constructs. Results are presented as fold of the empty vector and error bars are SEM. No significant differences were found between the tagged and untagged DVL1 constructs (one-way ANOVA, Tukey HSD tests, both *P*-values > 0.5).

6.8. Summary of the impact of mtDVL1 on canonical WNT signalling

The initial finding that at high levels of transfection *mtDVL1* was less active in the canonical WNT pathway than either *wtDVL1* or *shDVL1* (Figure 6.1) was unexpected as the phenotype seen in these individuals supports a gain-of-function increase in canonical WNT signalling (see Discussion and Introduction). The subsequent investigation into the sensitivity of each DVL1 construct to external WNT stimulus also indicated against our hypothesis of a gain-of-function increase in canonical WNT signalling from the mtDVL1. The *wtDVL1*, *mtDVL1*, and *shDVL1* when transfected all had a similar impact upon the C2C12's response to WNT stimulus (Figure 6.2), a response that appears to be largely independent of the exogenous *DVL1* (Figure 6.5). However when co-expressed with the *wtDVL1* the *mtDVL1* caused a substantial increase in canonical WNT activity (Figure 6.3). This result is particularly pertinent to the affected individuals as they are heterozygous for the mutations in *DVL1* and thus co-express mutant and wild type *DVL1*.

7. CHAPTER SEVEN - DISCUSSION

7.1. Robinow Syndrome phenotype

Apart from the osteosclerosis there are a number of other features consistently shared by the three cases studied here. The most striking of these is the oligodontia, which, at the severity shown here, is rare.[100] Oligodontia does occur in dominant RS without osteosclerosis, but in only about 10% of cases[9] whereas it occurred here in all three individuals studied here and one of the older cases from the literature[13] (Case 4, see Chapter 2). The role of canonical WNT in tooth agenesis is well established,[101] and thus the dysregulation of canonical WNT signalling which is implied by the skeletal phenotype may also explain the dental findings. Additionally hearing loss is a recurring symptom in all three cases, most reporting mixed bilateral sensorineural and conductive hearing loss. The recurrent otitis media could well be due to the osteosclerosis causing the eustachian tube to become obstructed (eustachian tube atresia was found in Case 3[93]), and in turn the conductive hearing loss will, in part, be due to the chronic otitis media. The sensorineural hearing loss may also be due to the osteosclerosis as it could compress the eighth cranial nerve (auditory) as it traverses the temporal bone and internal auditory canal.

7.2. Osteosclerotic phenotype

While there are a number of factors that cause osteosclerosis, the pattern of bone overgrowth in these individuals is similar to that found in the *LRP5* gain-of-function mutants, who have over active canonical WNT signalling.[51] In particular the generalised thickening of bone without an apparent rise in fragility (no history of unusual fractures in these individuals) is a strong parallel to these

mutations. This phenotype, in the context of recurrent *de novo* mutations in a WNT mediator, provides compelling evidence that this osteosclerosis is mediated by an increase in canonical WNT signalling.

7.3. Expression of mtDVL1

It is unlikely that the mutations in *DVL1* exert their effect through a simple loss-of-function. As discussed, no mouse knockouts of any DVL orthologue show osteosclerosis,[84] and of the three DVL null mice those lacking *Dvl1* have the mildest phenotype with no dysmorphic features.[25] and while the *Dvl2* and *3* null mice have a more severe phenotype (see Introduction) none display an RS-like phenotype or osteosclerosis[85,86]. In addition the database of human chromosomal abnormalities, DECIPHER,[92] catalogues no individuals who have deletions over the region containing *DVL1* as having similar features to the cases presented here. In order to investigate this gain-of-function hypothesis the expression of *mtDVL1* at the mRNA and protein level was investigated.

7.3.1. Expression of *mtDVL1* at the transcript level

Nonsense mediated decay (NMD) commonly leads to the degradation of transcripts possessing premature nonsense mutations.[102] We hypothesised that the transcripts with the *DVL1* mutations discussed here would resist NMD as the frameshift mutations do not lead to a premature nonsense codon before the last exon: NMD identifies aberrant transcripts by recognizing the exon junction complexes, allowing it to identify premature termination sequences if they fall before the last exon (NMD is reviewed in ref. [102]). Initially simply RT-PCR followed by Sanger sequencing was used to look for evidence that the transcripts generated from the mutant allele persisted. Accordingly a frameshifted trace was

found on the chromatogram indicating that the mutant allele was present. This was confirmed by restriction enzyme digest. The enzyme recognised a site in the *DVL1* transcript that was destroyed by the mutation, thus the mutant allele was resistant to its action. cDNA generated from fibroblasts from Case 1 showed a mixed population of *DVL1* transcripts, some of which were refractory to digestion, whereas a control digested to completion. It is not possible to be strictly quantitative from these results as the RT-PCR generated products form heteroduplices and any heteroduplex with the mutant site will resist the restriction digest. However, qualitatively, it is clear that there is a non-negligible amount of mtDVL1 mRNA and thus NMD was not degrading the mutant transcript.

It is worth noting that individuals with RS-OS are heterozygous, having both a wild type and mutated *DVL1* allele, the Sanger chromatogram and restriction digest detailed in Chapter 4 both confirmed that the mutant transcript was present alongside the wild type (the co-expression will be discussed later in this chapter).

7.3.2. Protein expression of mtDVL1

The original approach taken was to use endogenous lysate from the same population of cells from case 1 used to investigate the mRNA expression. As indicated in Chapter 4 there was a problem with a non-specific interaction of the commercial antibody. Unfortunately the cross-reactivity to a component of the cell culture media identified a band that was approximately the same molecular weight as DVL1 thus for some time this work proceeded under the assumption that DVL1 was being identified by Western blot. This led to the pursuit of a 2-D

gel electrophoretic method in an effort to use the differing charge to separate mutant from wild type protein. When the inefficacy of the antibody was identified well-validated DVL1 antibodies were sought from the literature. Almost exclusively they were directed towards C-terminal epitopes (as this is the most variable part of the DVLs, thus the best to distinguish the isoforms), and these were clearly of no help for this work because the mtDVL1 protein lacks the native DVL1 C-terminal.

7.3.3. DVL1 – differences in DVL1 protein levels

Using the transfected EGFP-DVL1 constructs it was shown that there was no significant difference in protein levels between the wtDVL1 and mtDVL1. This was indicated initially by the chemiluminescent Western blot (Figure 5.5) and then confirmed by the more quantitative results from the Odyssey (Figure 5.6). It is worth noting that a significant difference in protein level was found between the wtDVL1 and the shDVL1 (shDVL1 was ~2-fold wtDVL1), this, coupled with the non-significant increase in mtDVL1 will be discussed shortly.

There is a second product, which across the three experiments in Figure 5.6 occurs exclusively in the mtDVL1 (the second lower molecular weight band). In other Western blots (data not shown) a similar, albeit fainter, product has been seen in *wtDVL1* expression. This product is likely to be a C-terminal truncation, as clearly the N-terminal-EGFP-tag is still present (this is what the antibody detects). Further work would be required to better determine the nature of this product, but that is outside the scope of this thesis. As was presented in the results, if the second product is excluded from the quantification, the mtDVL1 protein level is still not lower than the wtDVL1 (it is ~1.2-fold). Thus these

results, irrespective of the second lower molecular weight product, confirm that the mtDVL1 protein is present at a similar level to wtDVL1, which is consistent with the proposed gain-of-function hypothesis.

7.3.4. Subtle regulation of DVL1 protein stability

The assay system used, with high levels of expression of DVL1 (100 ng/well transfected) may have been unable to pick up the subtle differences in DVL1 protein stability due to endogenous regulators (and this assay did detect an increase in the shDVL1 stability). There are four regulators of DVL stability that have binding sites that may be affected by the mutations: these are three ubiquitin ligases and a DVL degrading enzyme.

A proline motif (525-528, PPAY), within the region affected by the mutation, is the likely or confirmed binding site for three ubiquitin ligases: NEDL1,[76] ITCH,[77] and NEDD4L.[78] All three of these in co-expression with DVL have been shown to lead to DVL degradation (the critical domain, PPXY, is conserved throughout the DVL proteins). This degradation by ITCH and NEDD4L has been shown to directly negatively regulate canonical WNT signalling.[77,78] Negative regulation was not assessed for NEDL1.[76] Another, non-ubiquitinating, DVL regulator is guanine nucleotide binding protein β 2 ($G\beta_2$). This protein interacts with the DEP-C region of DVL (which includes the region altered by these mutations). In concert with its functional partner, $G\gamma_2$, this protein has both been shown to degrade DVL and through this degradation inhibit canonical WNT signalling.[79]

The mtDVL1 and shDVL1 are likely to be refractory to degradation by some or all of these mediators and future work could investigate the effect that these DVL1-interacting proteins have on the stability of mtDVL1 and shDVL1 through co-

transfection. However simply an increase in stability, and thus amount, of mtDVL1 over the wtDVL1 is not sufficient to explain the osteosclerotic phenotype. The supraphysiological expression of the mtDVL1 did not lead to an increase in canonical WNT signalling (see Figure 6.1), thus simply an accumulation of this mutant product does not, alone, explain the bone phenotype.

7.3.5. Subcellular localisation of mtDVL1

In order to signal in the canonical pathway DVL forms dynamic multimeric polymers via its DIX domain, in contrast to the original claim that the polymers were associations with cytoplasmic vesicles.[33] The ability to form these multimeric polymers was particularly relevant to the mtDVL1, as the polymers are required for canonical signalling, the formation of these puncta was required to support the hypothesised gain-of-function effect of these mutations.[88] The mtDVL1 and shDVL1 both possess DIX domains so it was likely that they would still polymerise. This was confirmed by this work which showed that the subcellular localisation of mtDVL1 and shDVL1 is similar to that of the wtDVL1, when examined by light microscopy.

7.4. Impact of DVL1 on canonical WNT signalling

7.4.1. Relationship between DVL1 transfection and WNT signalling

We found, as has been previously demonstrated,[80; 82] that DVL1 will increase canonical WNT signalling upon transient transfection in the absence of additional WNT stimulus. The results in Figure 6.1 showing the reduced function of the shDVL1 (with a C-terminal truncation) also align well with the literature,[80;

[82] however, in our experiments statistical significance between the activity of the shDVL1 and wtDVL1 was not reached. The most surprising result from our experiment however, was that the mtDVL1 was markedly less active than either the wild type or truncated forms. Essentially, after an apparent initial rise the mutant DVL1 failed to increase signalling at all. The mtDVL1 reduced impact on canonical WNT signalling compared to the wtDVL1 is unexpected given the osteosclerotic phenotype in the affected individuals but sits comfortably with the previous studies that have detailed the impact of DVL1 C-terminal truncation.[80; 82] The difference between the mtDVL1 and the shDVL1, however, indicates that this novel sequence is acting in a way that is distinct from merely the absence of C-terminal.

Initially it was suspected that this result indicated that the mtDVL1 construct was simply non-functional, plausibly because of some substantial misfolding impacting its expression (as occurs with *ROR2* mutations in recessive RS[19]). However the previously discussed work, which showed the pattern of mtDVL1 expression was similar to the wtDVL1 (Figure 5.4), and the work on protein stability (Figure 5.5 and Figure 5.6), indicated against this effect being mediated by the degradation or sequestration of the protein. It is also worth noting that the mutant protein does increase signalling above baseline, it just fails to increase this signalling with increasing expression, this will be discussed shortly. There are a number of possible DVL1 interactions that relate to the C-terminus and could explain our observations. These are discussed below.

It has been shown by Jung *et al*. that the C-terminal contains a site critical for the binding of a deubiquitinating enzyme (Usp14).[82] The mutation of just a few C-

terminal residues dramatically reduced the ability of DVL1 to signal in the canonical WNT pathway. In addition the Src family of tyrosine kinases, which are important for activation of WNT signalling downstream of DVL, bind to the C-terminal of DVL2 (broadly homologous to DVL1-C-terminal) alongside their SH-3 binding domain in a more N-terminal region.[72] A 2013 paper identified that the protein IQGAP1 will bind with the C-terminal of DVL1 (residues 476-671). A knockdown of IQGAP1 was found to reduce DVL1 nuclear localisation in response to WNT stimulus.[81] The nuclear localisation of DVL is a necessary step in canonical WNT signalling.[35]

The mtDVL1 lacks the residues (see Table 4.1 and Figure 4.2 for the affected regions of the mutant DVL1s across the Cases) for all three of these interactions, but so does the truncated form (shDVL1) Thus the above may well, to some degree, explain the observed reduced function of the mutant they do not explain the difference between mtDVL1 and shDVL1.

Work from Tauriello *et al.* on DVL1-Fz interaction does provide a possible explanation.[80] In this work, using a series of binding assays, it is shown that the wild type DVL1 interacts with the Fz using both the DEP domain and the C-terminal region (last 16 residues). A truncated form of DVL1 shows far weaker Fz binding. This novel C-terminal sequence is highly basic; it is therefore plausible that this new section of protein negatively affects the ability of the DVL1 to bind to the Fz, either simply sterically or due to its significant positive charge.

7.4.2. High levels of DVL1 transfection

There is some evidence from this project that very high levels of DVL1 expression may lead to a decline in canonical WNT activation. In the experiment investigating the impact of the EGFP tag (Figure 6.6) the *wtDVL1*, at 100 ng/well) only led to an ~8-fold increase over the empty vector, whereas at 32 ng/well an ~29-fold increase was observed (Figure 6.1). Additionally the *mtDVL1* at 100 ng/well was less active (~0.66-fold) than the empty vector (Figure 6.6), in contrast to its ~3.5-fold increase at 8 ng/well in Figure 6.1. This is only a preliminary indication, and further experimentation would be needed to confirm that, at high levels of DVL1 transfection, canonical WNT activation declines. This finding is of little currently apparent biological relevance, and peripheral to the aims of this thesis, but it may become relevant in future work.

7.4.3. Sensitivity to WNT stimulus and the WNT3A independence of *DVL1* signalling

The substantial increase seen in Figure 6.1 with wtDVL1 over-expression (and to a lesser extent with the shDVL1) is unlikely to represent a physiological property of DVL1, and this effect may well cloud other impacts of the mtDVL1 which are not simply mediated by the high expression level. Thus all future experiments focused at the lower level of DVL1 expression, 4 ng/well, a level at which the impact of DVL1 could still be observed over an empty vector.

Firstly a difference between the wtDVL1 and the mtDVL1 or shDVL1's sensitivity to WNT stimulus was investigated, and no difference was found (Figure 6.2). Interestingly it was observed that the impact of the DVL1 transfection on WNT signalling and the impact of WNT3A seemed to be mathematically independent

of each other. As more WNT3A conditioned media was added there was an increase in the canonical WNT activity in the cells transfected with *DVL1* constructs and the cells transfected with the empty vector (Figure 6.2 and Figure 6.4). While the cells transfected with *DVL1* showed a larger response to WNT3A stimulation than the empty vector cells in an absolute sense the rate of increase was the same in the cells with and without transfected *DVL1* (Figure 6.5).

As stated in the results this is an example of statistical independence, i.e. the *DVL1* transfection does not, at this level, change the response to WNT3A stimulus. It was suspected that DVL1, as a component of the canonical WNT cascade, would potentiate the response to WNT3A stimulus but this did not occur. This implies that the *DVL1* transfection is increasing canonical WNT activity in a WNT-ligand independent manner – i.e. the DVL1 increases the activity in canonical WNT pathway to the same degree regardless of the amount of extracellular WNT-ligand. It is worth noting that the C2C12 cells will express endogenous *Dvl1* (they are a mouse cell line) and that the DMEM that the cells are cultured in (see Methods) is likely to contain WNT ligand, thus more work would be required to fully analyse this relationship. However the ability of DVL1 to signal without WNT-ligand (which would be consistent with the above result) is an interesting hypothesis, which could be investigated in future work.

7.4.4. Synergy when mtDVL1 and wtDVL1 are co-expressed

When the *mtDVL1* allele is expressed *in trans* (as it is in these heterozygous cases) with the *wtDVL1* allele it has quite a dramatic effect on canonical WNT signalling (at 4 ng total *DVL1*/well) where it raises the activity three fold over that of *wtDVL1* expressed alone (Figure 6.3). This rise in activity is maintained in

the presence of WNT3A stimulation (Figure 6.4). This may well explain the initial rise observed when mtDVL1 was transfected at low levels into C2C12 cells (Figure 6.1), this could result from a synergy with the endogenously expressed mouse *Dvl1*. A possible explanation of this interaction lies in DVL1 phosphorylation.

DVLs are phosphorylated in response to both canonical and non-canonical WNT stimulus.[103] In particular Casein Kinases-1 (CK1) ϵ has proved to be an important mediator of DVL phosphorylation.[70,75] Phosphorylation leads to an inactive form of DVL as shown by its inability to self-associate to form puncta.[70,75] Puncta are known to be critical to the ability of DVL to signal in the canonical pathway.[34] Bernatik *et al*.[70] found that CK1ϵ over-expression would phosphorylate wild type and C-terminal truncated DVL (DVL-ΔC – the construct was produced from a His502* mutant, which is very similar to our shDVL1's Trp507* mutation) to the same degree. However the C-terminal deleted DVL remained self-associated in puncta after CK1ϵ addition, in contrast to the wild type DVL which dispersed in response to CK1ϵ. A subsequent paper[75] found that if CK1ϵ was only present at endogenous levels (rather than the excess used by Bernatik *et al*.) it would not phosphorylate a DVL that lacked three critical C-terminal Ser and Thr residues.[75] These residues are conserved across the DVLs but absent from our mutants (in DVL1 they are Ser553, Thr554, and Ser556). This led to the conclusion that the effect observed by Bernatik *et al*. was likely due to over-expression of CK1ϵ, which was consistent with initial finding from Bernatik *et al*. that the DVL-ΔC would not pull down endogenous CK1ϵ.

Thus the CK1ϵ phosphorylation of DVL is a negative feedback on DVL function in the canonical WNT pathway. Either the CK1ϵ phosphorylation requires C-terminal residues which are not present in the mutant,[75] or the mechanism by which the phosphorylated DVL inhibits canonical signalling depends upon the C-terminal itself.[70] It is therefore plausible that the mutant resists this negative feedback. In particular the persistence of the mutant in an unphosphorylated state may allow it to stabilise the DVL1 puncta that are necessary for canonical signalling even though it seems to be inactive in the canonical WNT signalling pathway itself (Figure 6.1). There is some additional supporting evidence for this from the literature. Using a DVL2 construct that was mutated at these three key phosphorylated residues (but otherwise possessed a normal C-terminal) Gonzalez-Sancho *et al.*[75] found that the canonical WNT activity of their mutant was identical to wild type DVL2 activity, except at the low levels of transfection where it was found that the "unphosphorylatable" construct was more active than wtDVL2. The work in this thesis indicates that this may have been due to an interaction with endogenous DVL, and that they may have found the same 'synergy' we observed (note that their construct possessed an otherwise normal C-terminal, hence it still functioned in the canonical pathway at high levels of expression).

This model of phosphorylation does not however completely explain the observation as it does not account for the difference between the *mtDVL1* and *shDVL1* when co-transfected with the *wtDVL1*. The *sh/wtDVL1* transfection was not significantly different from the *wtDVL1* alone, however it is worth noting that the *P*-value in the absence of WNT3A stimulation was ~0.15 so perhaps there is

a difference here that this work lacked the power to detect. That aside there is a difference between how the mtDVL1 and shDVL1 proteins behave in the presence of wtDVL1. Clearly the novel sequence has some new function, but as of yet there is no apparent explanation. It seems to be no coincidence that all three individuals not only lack the wild type DVL1 C-terminus in their mutant DVL1 but also have the same novel sequence.

7.5. Mutant DVL1 in PCP/WNT signalling

As is discussed the DVLs are important canonical and non-canonical WNT mediators. The relationship between RS and non-canonical/PCP WNT signalling is robust, as previously discussed in the Introduction. During this project zebrafish were considered as a potential model of RS which would allow the investigation of the impact of the mutant DVL1. Zebrafish have previously been used to model PCP phenotypes,[104] it is possible to observe shorter and broader somites, shortened A-P axis, and undulations in the notochord. For this thesis however this method proved unlikely to be applicable, notably because PCP signalling is gradient dependent and inhibition and activation of the pathway can yield the same phenotype[43] (as considered in the Introduction). In a practical sense this meant that injection of both normal human *DVL1* RNA and the mutation-bearing *DVL1* RNA would disrupt PCP/WNT (this was done during the course of this study, but the results are preliminary, thus not included in this thesis). It was thought unlikely that there would be an easily identifiable difference between mutant and wild type *DVL1* expression in the fish. In future use of *in vivo* targeted genetic mutation systems such as a CRISPR/Cas9 or TALENs could enable a study of this phenotype in an animal model.

The genetics provide very compelling evidence that the mutations described here are causative of RS in these patients. RS is a rare condition with only around 100 cases in the literature in total, so the probability of finding such a similar mutation in three unrelated patients with RS, if it were not causative, is minuscule.

This thesis has provided good evidence that in the canonical/β-catenin pathway the mtDVL1 is a gain-of-function (expression data from

Figure 4.3, Figure 4.4 and Figure 4.5 and the activating interaction with wtDVL1 in Figure 6.3 and Figure 6.4) and the same may be true with the impact on the PCP/WNT. This is in contrast to our hypothesis at the outset of this project that the impact upon the PCP/WNT pathway was likely to be a loss-of-function, in line with the demonstrated loss-of-function mutations in *WNT5A*[20] and *ROR2*[14; 15]which are known to cause RS (see Introduction).

Further research identified that the mouse knockout of *Dvl1* which no physical phenotype,[25] and, given the conservation of DVL1 across species,[66] it is likely that these mice provide a good model for human loss-of-function. Additionally the database of chromosomal abnormalities, DECIPHER, does not identify RS in patients who lack a copy of *DVL1*. Therefore a simple loss-of-function is unlikely to explain the RS in these patients, and, perhaps the action of the mutant *DVL1* may be better considered as a disruption of PCP/WNT signalling (as considered in the Introduction). There are a number of important PCP/WNT mediators that interact with the C-terminal of DVL in particular PRICKLE1 and ROR2, which are discussed below. These both provide hypothetical mechanisms which could

explain this likely PCP/WNT defect, but future laboratory work is now required to further study the RS phenotype in these patients.

7.5.1. Mutant DVL1-PRICKLE

Prickle-DVL interaction is an interesting target as mice with null and hypomorphic *Prickle1* alleles phenocopy human RS,[23] and *Drosophila* prickle has been shown to interact with the DEP-C-terminal aspect of dsh (the protein sequence of which is strongly conserved in humans[66]).[105] Of particular note it was found that the absence of prickle in mice led to the complete loss of Dvl2 polarisation in chondrocytes (normally a critical part of PCP/WNT signalling) in the Robinow-like mice.[23] One possible model is that the mtDVL1 fails to interact with PRICKLE1, thus does not polarise in response to PCP/WNT signalling, therefore disrupting the PCP gradient.

7.5.2. Mutant DVL1-ROR2

ROR2 is an integral part of the PCP pathway,[30] and mutations in *ROR2* can cause a Robinow Syndrome phenotype in humans and mice.[15,14] It has been shown that mouse Ror2 (mouse) will interact with DVL3 (human) through the C-terminus, and that this interaction will inhibit canonical/β-catenin WNT activity (one of the known actions of the PCP pathway[30]).[83] Thus another possible mechanism is that either the absence of C-terminal precludes ROR2 binding, or even that the new C-terminal interacts with ROR2 in some way to enhance PCP/WNT signalling. A consideration with this information is that this work was done with DVL3, which, while still heavily conserved, has the most atypical C-terminal of the DVLs,[74] thus the possibility that the effect observed by the authors is unique to DVL3 cannot be dismissed.

7.6. Mutant DVL1 in Ca^{2+}-dependent WNT signalling

As detailed in the introduction there is another non-canonical WNT pathway that signals through changing the intracellular Ca^{2+} concentration. This pathway is sometimes considered a component of the PCP pathway (but is not in this thesis) as WNT5A also stimulates it[44,45], but it is less well characterized than the PCP pathway (it is reviewed in ref. 46). As discussed in the Introduction DVL plays an important, and complex, role in this pathway by both inhibiting and activating Ca^{2+}/WNT.[47; 48] The impact of the mutation on Ca^{2+}/WNT signalling has not been assessed largely because defects in Ca^{2+} dependent WNT signalling have not been associated with the clinical features in these individuals (namely RS and this pattern of osteosclerosis). This could be an area of future work.

7.7. Conclusions

This work places mutations in *DVL1* alongside *ROR2* and *WNT5A* as causative of RS. These mutations cause a particular novel subtype of RS, that we have named RS-OS. The *DVL1* mutations almost certainly act by affecting the PCP/WNT pathway (RS) and the canonical WNT pathway (osteosclerosis), and this thesis has elucidated the mechanism by which these mutations affect the latter. This work has shown that the mutant transcript persists in endogenous cells and that the protein is expressed, stable, and localises in a similar manner to wild type DVL1, supporting a gain-of-function. The subsequent work with the TOPFlash luciferase assays showed that these mutant alleles act in part through their novel C-terminal sequence and only increase canonical WNT signalling in concert with the wild type. The mechanism by which the mutant *DVL1* effects canonical WNT signalling remains to be elucidated, but a gain-of-function mutation that relies

upon the presence of the wild type allele to act is, to the best of our knowledge, unique amongst Mendelian disorders. Given that these affected individuals are heterozygotes, co-expressing mutant and wild type *DVL1* alleles, this work supports the hypothesis that the osteosclerotic phenotype is due to an increase in canonical WNT signalling.

8. REFERENCES

1. Bunn, K.J., Lai, A., Al-Ani, A., Farella, M., Craw, S., and Robertson, S.P. (2014). An osteosclerotic form of Robinow syndrome. American journal of medical genetics Part A.
2. Van Buchem, F.S., Hadders, H.N., and Ubbens, R. (1955). An uncommon familial systemic disease of the skeleton: hyperostosis corticalis generalisata familiaris. Acta radiologica 44, 109-120.
3. Balemans, W., Patel, N., Ebeling, M., Van Hul, E., Wuyts, W., Lacza, C., Dioszegi, M., Dikkers, F.G., Hildering, P., Willems, P.J., et al. (2002). Identification of a 52 kb deletion downstream of the SOST gene in patients with van Buchem disease. Journal of medical genetics 39, 91-97.
4. Li, X., Zhang, Y., Kang, H., Liu, W., Liu, P., Zhang, J., Harris, S.E., and Wu, D. (2005). Sclerostin binds to LRP5/6 and antagonizes canonical Wnt signaling. The Journal of biological chemistry 280, 19883-19887.
5. Semenov, M., Tamai, K., and He, X. (2005). SOST is a ligand for LRP5/LRP6 and a Wnt signaling inhibitor. The Journal of biological chemistry 280, 26770-26775.
6. Robinow, M., Silverman, F.N., and Smith, H.D. (1969). A newly recognized dwarfing syndrome. Am J Dis Child 117, 645-651.
7. Wadia, R.S., Shirole, D.B., and Dikshit, M.S. (1978). Recessively inherited costovertebral segmentation defect with mesomelia and peculiar facies (Covesdem syndrome): A new genetic entity? Journal of medical genetics 15, 123-127.
8. Wadia, R.S. (1979). Covesdem syndrome. Journal of medical genetics 16, 162.
9. Mazzeu, J.F., Pardono, E., Vianna-Morgante, A.M., Richieri-Costa, A., Ae Kim, C., Brunoni, D., Martelli, L., de Andrade, C.E., Colin, G., and Otto, P.A. (2007). Clinical characterization of autosomal dominant and recessive variants of Robinow syndrome. American journal of medical genetics Part A 143, 320-325.
10. Bain, M.D., Winter, R.M., and Burn, J. (1986). Robinow syndrome without mesomelic 'brachymelia': a report of five cases. Journal of medical genetics 23, 350-354.
11. Al Kaissi, A., Bieganski, T., Baranska, D., Chehida, F.B., Gharbi, H., Ghachem, M.B., Hendaoui, L., Safi, H., and Kozlowski, K. (2007). Robinow syndrome: report of two cases and review of the literature. Australasian radiology 51, 83-86.
12. Shprintzen, R.J., Goldberg, R.B., Saenger, P., and Sidoti, E.J. (1982). Male-to-male transmission of Robinow's syndrome. Its occurrence in association with cleft lip and cleft palate. American journal of diseases of children 136, 594-597.
13. Kelly, T.E., Benson, R., Temtamy, S., Plotnick, L., and Levin, S. (1975). The Robinow syndrome: an isolated case with a detailed study of the phenotype. American journal of diseases of children 129, 383-386.
14. van Bokhoven, H., Celli, J., Kayserili, H., van Beusekom, E., Balci, S., Brussel, W., Skovby, F., Kerr, B., Percin, E.F., Akarsu, N., et al. (2000). Mutation of the gene encoding the ROR2 tyrosine kinase causes autosomal recessive Robinow syndrome. Nature genetics 25, 423-426.
15. Afzal, A.R., Rajab, A., Fenske, C.D., Oldridge, M., Elanko, N., Ternes-Pereira, E., Tuysuz, B., Murday, V.A., Patton, M.A., Wilkie, A.O., et al. (2000). Recessive

Robinow syndrome, allelic to dominant brachydactyly type B, is caused by mutation of ROR2. Nature genetics 25, 419-422.
16. Oldridge, M., Fortuna, A.M., Maringa, M., Propping, P., Mansour, S., Pollitt, C., DeChiara, T.M., Kimble, R.B., Valenzuela, D.M., Yancopoulos, G.D., et al. (2000). Dominant mutations in ROR2, encoding an orphan receptor tyrosine kinase, cause brachydactyly type B. Nature genetics 24, 275-278.
17. Schwabe, G.C., Tinschert, S., Buschow, C., Meinecke, P., Wolff, G., Gillessen-Kaesbach, G., Oldridge, M., Wilkie, A.O., Komec, R., and Mundlos, S. (2000). Distinct mutations in the receptor tyrosine kinase gene ROR2 cause brachydactyly type B. American journal of human genetics 67, 822-831.
18. Afzal, A.R., and Jeffery, S. (2003). One gene, two phenotypes: ROR2 mutations in autosomal recessive Robinow syndrome and autosomal dominant brachydactyly type B. Human mutation 22, 1-11.
19. Chen, Y., Bellamy, W.P., Seabra, M.C., Field, M.C., and Ali, B.R. (2005). ER-associated protein degradation is a common mechanism underpinning numerous monogenic diseases including Robinow syndrome. Human molecular genetics 14, 2559-2569.
20. Person, A.D., Beiraghi, S., Sieben, C.M., Hermanson, S., Neumann, A.N., Robu, M.E., Schleiffarth, J.R., Billington, C.J., Jr., van Bokhoven, H., Hoogeboom, J.M., et al. (2010). WNT5A mutations in patients with autosomal dominant Robinow syndrome. Developmental dynamics : an official publication of the American Association of Anatomists 239, 327-337.
21. Schwabe, G.C., Trepczik, B., Suring, K., Brieske, N., Tucker, A.S., Sharpe, P.T., Minami, Y., and Mundlos, S. (2004). Ror2 knockout mouse as a model for the developmental pathology of autosomal recessive Robinow syndrome. Developmental dynamics : an official publication of the American Association of Anatomists 229, 400-410.
22. Yamaguchi, T.P., Bradley, A., McMahon, A.P., and Jones, S. (1999). A Wnt5a pathway underlies outgrowth of multiple structures in the vertebrate embryo. Development 126, 1211-1223.
23. Liu, C., Lin, C., Gao, C., May-Simera, H., Swaroop, A., and Li, T. (2014). Null and hypomorph Prickle1 alleles in mice phenocopy human Robinow syndrome and disrupt signaling downstream of Wnt5a. Biology open.
24. Yang, T., Jia, Z., Bryant-Pike, W., Chandrasekhar, A., Murray, J.C., Fritzsch, B., and Bassuk, A.G. (2014). Analysis of PRICKLE1 in human cleft palate and mouse development demonstrates rare and common variants involved in human malformations. Molecular genetics & genomic medicine 2, 138-151.
25. Lijam, N., Paylor, R., McDonald, M.P., Crawley, J.N., Deng, C.X., Herrup, K., Stevens, K.E., Maccaferri, G., McBain, C.J., Sussman, D.J., et al. (1997). Social interaction and sensorimotor gating abnormalities in mice lacking Dvl1. Cell 90, 895-905.
26. Clevers, H. (2006). Wnt/beta-catenin signaling in development and disease. Cell 127, 469-480.
27. Kikuchi, A., Yamamoto, H., Sato, A., and Matsumoto, S. (2011). New insights into the mechanism of Wnt signaling pathway activation. International review of cell and molecular biology 291, 21-71.
28. Niehrs, C. (2012). The complex world of WNT receptor signalling. Nature reviews Molecular cell biology 13, 767-779.

29. Rijsewijk, F., Schuermann, M., Wagenaar, E., Parren, P., Weigel, D., and Nusse, R. (1987). The Drosophila homolog of the mouse mammary oncogene int-1 is identical to the segment polarity gene wingless. Cell 50, 649-657.
30. Oishi, I., Suzuki, H., Onishi, N., Takada, R., Kani, S., Ohkawara, B., Koshida, I., Suzuki, K., Yamada, G., Schwabe, G.C., et al. (2003). The receptor tyrosine kinase Ror2 is involved in non-canonical Wnt5a/JNK signalling pathway. Genes to cells : devoted to molecular & cellular mechanisms 8, 645-654.
31. Smallwood, P.M., Williams, J., Xu, Q., Leahy, D.J., and Nathans, J. (2007). Mutational analysis of Norrin-Frizzled4 recognition. The Journal of biological chemistry 282, 4057-4068.
32. Kazanskaya, O., Glinka, A., del Barco Barrantes, I., Stannek, P., Niehrs, C., and Wu, W. (2004). R-Spondin2 is a secreted activator of Wnt/beta-catenin signaling and is required for Xenopus myogenesis. Developmental cell 7, 525-534.
33. Schwarz-Romond, T., Merrifield, C., Nichols, B.J., and Bienz, M. (2005). The Wnt signalling effector Dishevelled forms dynamic protein assemblies rather than stable associations with cytoplasmic vesicles. Journal of cell science 118, 5269-5277.
34. Schwarz-Romond, T., Fiedler, M., Shibata, N., Butler, P.J., Kikuchi, A., Higuchi, Y., and Bienz, M. (2007). The DIX domain of Dishevelled confers Wnt signaling by dynamic polymerization. Nature structural & molecular biology 14, 484-492.
35. Itoh, K., Brott, B.K., Bae, G.U., Ratcliffe, M.J., and Sokol, S.Y. (2005). Nuclear localization is required for Dishevelled function in Wnt/beta-catenin signaling. Journal of biology 4, 3.
36. Shulman, J.M., Perrimon, N., and Axelrod, J.D. (1998). Frizzled signaling and the developmental control of cell polarity. Trends in genetics : TIG 14, 452-458.
37. Gao, C., and Chen, Y.G. (2010). Dishevelled: The hub of Wnt signaling. Cellular signalling 22, 717-727.
38. Veeman, M.T., Axelrod, J.D., and Moon, R.T. (2003). A second canon. Functions and mechanisms of beta-catenin-independent Wnt signaling. Developmental cell 5, 367-377.
39. Habas, R., Kato, Y., and He, X. (2001). Wnt/Frizzled activation of Rho regulates vertebrate gastrulation and requires a novel Formin homology protein Daam1. Cell 107, 843-854.
40. Winter, C.G., Wang, B., Ballew, A., Royou, A., Karess, R., Axelrod, J.D., and Luo, L. (2001). Drosophila Rho-associated kinase (Drok) links Frizzled-mediated planar cell polarity signaling to the actin cytoskeleton. Cell 105, 81-91.
41. Rosso, S.B., Sussman, D., Wynshaw-Boris, A., and Salinas, P.C. (2005). Wnt signaling through Dishevelled, Rac and JNK regulates dendritic development. Nature neuroscience 8, 34-42.
42. Ho, H.Y., Susman, M.W., Bikoff, J.B., Ryu, Y.K., Jonas, A.M., Hu, L., Kuruvilla, R., and Greenberg, M.E. (2012). Wnt5a-Ror-Dishevelled signaling constitutes a core developmental pathway that controls tissue morphogenesis. Proceedings of the National Academy of Sciences of the United States of America 109, 4044-4051.

43. Goto, T., and Keller, R. (2002). The planar cell polarity gene strabismus regulates convergence and extension and neural fold closure in Xenopus. Developmental biology 247, 165-181.
44. Slusarski, D.C., Yang-Snyder, J., Busa, W.B., and Moon, R.T. (1997). Modulation of embryonic intracellular Ca2+ signaling by Wnt-5A. Developmental biology 182, 114-120.
45. Slusarski, D.C., Corces, V.G., and Moon, R.T. (1997). Interaction of Wnt and a Frizzled homologue triggers G-protein-linked phosphatidylinositol signalling. Nature 390, 410-413.
46. De, A. (2011). Wnt/Ca2+ signaling pathway: a brief overview. Acta biochimica et biophysica Sinica 43, 745-756.
47. Sheldahl, L.C., Slusarski, D.C., Pandur, P., Miller, J.R., Kuhl, M., and Moon, R.T. (2003). Dishevelled activates Ca2+ flux, PKC, and CamKII in vertebrate embryos. The Journal of cell biology 161, 769-777.
48. Kilander, M.B., Petersen, J., Andressen, K.W., Ganji, R.S., Levy, F.O., Schuster, J., Dahl, N., Bryja, V., and Schulte, G. (2014). Disheveled regulates precoupling of heterotrimeric G proteins to Frizzled 6. FASEB journal : official publication of the Federation of American Societies for Experimental Biology 28, 2293-2305.
49. Wang, Y., Li, Y.P., Paulson, C., Shao, J.Z., Zhang, X., Wu, M., and Chen, W. (2014). Wnt and the Wnt signaling pathway in bone development and disease. Frontiers in bioscience 19, 379-407.
50. Brunkow, M.E., Gardner, J.C., Van Ness, J., Paeper, B.W., Kovacevich, B.R., Proll, S., Skonier, J.E., Zhao, L., Sabo, P.J., Fu, Y., et al. (2001). Bone dysplasia sclerosteosis results from loss of the SOST gene product, a novel cystine knot-containing protein. American journal of human genetics 68, 577-589.
51. Little, R.D., Carulli, J.P., Del Mastro, R.G., Dupuis, J., Osborne, M., Folz, C., Manning, S.P., Swain, P.M., Zhao, S.C., Eustace, B., et al. (2002). A mutation in the LDL receptor-related protein 5 gene results in the autosomal dominant high-bone-mass trait. American journal of human genetics 70, 11-19.
52. Hartikka, H., Makitie, O., Mannikko, M., Doria, A.S., Daneman, A., Cole, W.G., Ala-Kokko, L., and Sochett, E.B. (2005). Heterozygous mutations in the LDL receptor-related protein 5 (LRP5) gene are associated with primary osteoporosis in children. Journal of bone and mineral research : the official journal of the American Society for Bone and Mineral Research 20, 783-789.
53. Crabbe, P., Balemans, W., Willaert, A., van Pottelbergh, I., Cleiren, E., Coucke, P.J., Ai, M., Goemaere, S., van Hul, W., de Paepe, A., et al. (2005). Missense mutations in LRP5 are not a common cause of idiopathic osteoporosis in adult men. Journal of bone and mineral research : the official journal of the American Society for Bone and Mineral Research 20, 1951-1959.
54. Gong, Y., Slee, R.B., Fukai, N., Rawadi, G., Roman-Roman, S., Reginato, A.M., Wang, H., Cundy, T., Glorieux, F.H., Lev, D., et al. (2001). LDL receptor-related protein 5 (LRP5) affects bone accrual and eye development. Cell 107, 513-523.
55. Boudin, E., Steenackers, E., de Freitas, F., Nielsen, T.L., Andersen, M., Brixen, K., Van Hul, W., and Piters, E. (2013). A common LRP4 haplotype is

associated with bone mineral density and hip geometry in men-data from the Odense Androgen Study (OAS). Bone 53, 414-420.
56. Takada, I., Mihara, M., Suzawa, M., Ohtake, F., Kobayashi, S., Igarashi, M., Youn, M.Y., Takeyama, K., Nakamura, T., Mezaki, Y., et al. (2007). A histone lysine methyltransferase activated by non-canonical Wnt signalling suppresses PPAR-gamma transactivation. Nature cell biology 9, 1273-1285.
57. Kibar, Z., Torban, E., McDearmid, J.R., Reynolds, A., Berghout, J., Mathieu, M., Kirillova, I., De Marco, P., Merello, E., Hayes, J.M., et al. (2007). Mutations in VANGL1 associated with neural-tube defects. The New England journal of medicine 356, 1432-1437.
58. Kibar, Z., Salem, S., Bosoi, C.M., Pauwels, E., De Marco, P., Merello, E., Bassuk, A.G., Capra, V., and Gros, P. (2011). Contribution of VANGL2 mutations to isolated neural tube defects. Clinical genetics 80, 76-82.
59. Bosoi, C.M., Capra, V., Allache, R., Trinh, V.Q., De Marco, P., Merello, E., Drapeau, P., Bassuk, A.G., and Kibar, Z. (2011). Identification and characterization of novel rare mutations in the planar cell polarity gene PRICKLE1 in human neural tube defects. Human mutation 32, 1371-1375.
60. De Marco, P., Merello, E., Rossi, A., Piatelli, G., Cama, A., Kibar, Z., and Capra, V. (2012). FZD6 is a novel gene for human neural tube defects. Human mutation 33, 384-390.
61. De Marco, P., Merello, E., Consales, A., Piatelli, G., Cama, A., Kibar, Z., and Capra, V. (2013). Genetic analysis of disheveled 2 and disheveled 3 in human neural tube defects. Journal of molecular neuroscience : MN 49, 582-588.
62. Cai, C., and Shi, O. (2014). Genetic evidence in planar cell polarity signaling pathway in human neural tube defects. Frontiers of medicine 8, 68-78.
63. Yu, H.C., Wu, T.C., Chen, M.R., Liu, S.W., Chen, J.H., and Lin, K.M. (2010). Mechanical stretching induces osteoprotegerin in differentiating C2C12 precursor cells through noncanonical Wnt pathways. Journal of bone and mineral research : the official journal of the American Society for Bone and Mineral Research 25, 1128-1137.
64. Kaneuji, T., Ariyoshi, W., Okinaga, T., Toshinaga, A., Takahashi, T., and Nishihara, T. (2011). Mechanisms involved in regulation of osteoclastic differentiation by mechanical stress-loaded osteoblasts. Biochemical and biophysical research communications 408, 103-109.
65. Klingensmith, J., Nusse, R., and Perrimon, N. (1994). The Drosophila segment polarity gene dishevelled encodes a novel protein required for response to the wingless signal. Genes & development 8, 118-130.
66. Dillman, A.R., Minor, P.J., and Sternberg, P.W. (2013). Origin and evolution of dishevelled. G3 3, 251-262.
67. Lee, Y.N., Gao, Y., and Wang, H.Y. (2008). Differential mediation of the Wnt canonical pathway by mammalian Dishevelleds-1, -2, and -3. Cellular signalling 20, 443-452.
68. Sun, T.Q., Lu, B., Feng, J.J., Reinhard, C., Jan, Y.N., Fantl, W.J., and Williams, L.T. (2001). PAR-1 is a Dishevelled-associated kinase and a positive regulator of Wnt signalling. Nature cell biology 3, 628-636.
69. Willert, K., Brink, M., Wodarz, A., Varmus, H., and Nusse, R. (1997). Casein kinase 2 associates with and phosphorylates dishevelled. The EMBO journal 16, 3089-3096.

70. Bernatik, O., Ganji, R.S., Dijksterhuis, J.P., Konik, P., Cervenka, I., Polonio, T., Krejci, P., Schulte, G., and Bryja, V. (2011). Sequential activation and inactivation of Dishevelled in the Wnt/beta-catenin pathway by casein kinases. The Journal of biological chemistry 286, 10396-10410.
71. Penton, A., Wodarz, A., and Nusse, R. (2002). A mutational analysis of dishevelled in Drosophila defines novel domains in the dishevelled protein as well as novel suppressing alleles of axin. Genetics 161, 747-762.
72. Yokoyama, N., and Malbon, C.C. (2009). Dishevelled-2 docks and activates Src in a Wnt-dependent manner. Journal of cell science 122, 4439-4451.
73. Ma, L., Wang, Y., Malbon, C.C., and Wang, H.Y. (2010). Dishevelled-3 C-terminal His single amino acid repeats are obligate for Wnt5a activation of non-canonical signaling. Journal of molecular signaling 5, 19.
74. Wang, H.Y., and Malbon, C.C. (2012). Dishevelled C-terminus: prolyl and histidinyl motifs. Acta physiologica 204, 65-73.
75. Gonzalez-Sancho, J.M., Greer, Y.E., Abrahams, C.L., Takigawa, Y., Baljinnyam, B., Lee, K.H., Lee, K.S., Rubin, J.S., and Brown, A.M. (2013). Functional consequences of Wnt-induced dishevelled 2 phosphorylation in canonical and noncanonical Wnt signaling. The Journal of biological chemistry 288, 9428-9437.
76. Miyazaki, K., Fujita, T., Ozaki, T., Kato, C., Kurose, Y., Sakamoto, M., Kato, S., Goto, T., Itoyama, Y., Aoki, M., et al. (2004). NEDL1, a novel ubiquitin-protein isopeptide ligase for dishevelled-1, targets mutant superoxide dismutase-1. The Journal of biological chemistry 279, 11327-11335.
77. Wei, W., Li, M., Wang, J., Nie, F., and Li, L. (2012). The E3 ubiquitin ligase ITCH negatively regulates canonical Wnt signaling by targeting dishevelled protein. Molecular and cellular biology 32, 3903-3912.
78. Ding, Y., Zhang, Y., Xu, C., Tao, Q.H., and Chen, Y.G. (2013). HECT domain-containing E3 ubiquitin ligase NEDD4L negatively regulates Wnt signaling by targeting dishevelled for proteasomal degradation. The Journal of biological chemistry 288, 8289-8298.
79. Jung, H., Kim, H.J., Lee, S.K., Kim, R., Kopachik, W., Han, J.K., and Jho, E.H. (2009). Negative feedback regulation of Wnt signaling by Gbetagamma-mediated reduction of Dishevelled. Experimental & molecular medicine 41, 695-706.
80. Tauriello, D.V., Jordens, I., Kirchner, K., Slootstra, J.W., Kruitwagen, T., Bouwman, B.A., Noutsou, M., Rudiger, S.G., Schwamborn, K., Schambony, A., et al. (2012). Wnt/beta-catenin signaling requires interaction of the Dishevelled DEP domain and C terminus with a discontinuous motif in Frizzled. Proceedings of the National Academy of Sciences of the United States of America 109, E812-820.
81. Goto, T., Sato, A., Shimizu, M., Adachi, S., Satoh, K., Iemura, S., Natsume, T., and Shibuya, H. (2013). IQGAP1 functions as a modulator of dishevelled nuclear localization in Wnt signaling. PloS one 8, e60865.
82. Jung, H., Kim, B.G., Han, W.H., Lee, J.H., Cho, J.Y., Park, W.S., Maurice, M.M., Han, J.K., Lee, M.J., Finley, D., et al. (2013). Deubiquitination of Dishevelled by Usp14 is required for Wnt signaling. Oncogenesis 2, e64.
83. Witte, F., Bernatik, O., Kirchner, K., Masek, J., Mahl, A., Krejci, P., Mundlos, S., Schambony, A., Bryja, V., and Stricker, S. (2010). Negative regulation of

Wnt signaling mediated by CK1-phosphorylated Dishevelled via Ror2. FASEB journal : official publication of the Federation of American Societies for Experimental Biology 24, 2417-2426.
84. Wynshaw-Boris, A. (2012). Dishevelled: in vivo roles of a multifunctional gene family during development. Current topics in developmental biology 101, 213-235.
85. Hamblet, N.S., Lijam, N., Ruiz-Lozano, P., Wang, J., Yang, Y., Luo, Z., Mei, L., Chien, K.R., Sussman, D.J., and Wynshaw-Boris, A. (2002). Dishevelled 2 is essential for cardiac outflow tract development, somite segmentation and neural tube closure. Development 129, 5827-5838.
86. Etheridge, S.L., Ray, S., Li, S., Hamblet, N.S., Lijam, N., Tsang, M., Greer, J., Kardos, N., Wang, J., Sussman, D.J., et al. (2008). Murine dishevelled 3 functions in redundant pathways with dishevelled 1 and 2 in normal cardiac outflow tract, cochlea, and neural tube development. PLoS genetics 4, e1000259.
87. Wang, J., Hamblet, N.S., Mark, S., Dickinson, M.E., Brinkman, B.C., Segil, N., Fraser, S.E., Chen, P., Wallingford, J.B., and Wynshaw-Boris, A. (2006). Dishevelled genes mediate a conserved mammalian PCP pathway to regulate convergent extension during neurulation. Development 133, 1767-1778.
88. Bedell, J.A., Wagner-McPherson, C. B., Bengtsson, U., Handa, K., Dumars, K. W., Marsh, J. L., Smith, M., McPherson, J. D. (1996). A 1p deletion syndrome patient is hemizygous for a human homologue of the Drosophila dishevelled gene. (Abstract). Am J Hum Genet 59.
89. Windpassinger, C., Kroisel, P.M., Wagner, K., and Petek, E. (2002). The human gamma-aminobutyric acid A receptor delta (GABRD) gene: molecular characterisation and tissue-specific expression. Gene 292, 25-31.
90. Rosenfeld, J.A., Crolla, J.A., Tomkins, S., Bader, P., Morrow, B., Gorski, J., Troxell, R., Forster-Gibson, C., Cilliers, D., Hislop, R.G., et al. (2010). Refinement of causative genes in monosomy 1p36 through clinical and molecular cytogenetic characterization of small interstitial deletions. American journal of medical genetics Part A 152A, 1951-1959.
91. Arndt, A.K., Schafer, S., Drenckhahn, J.D., Sabeh, M.K., Plovie, E.R., Caliebe, A., Klopocki, E., Musso, G., Werdich, A.A., Kalwa, H., et al. (2013). Fine mapping of the 1p36 deletion syndrome identifies mutation of PRDM16 as a cause of cardiomyopathy. American journal of human genetics 93, 67-77.
92. Firth, H.V., Richards, S.M., Bevan, A.P., Clayton, S., Corpas, M., Rajan, D., Van Vooren, S., Moreau, Y., Pettett, R.M., and Carter, N.P. (2009). DECIPHER: Database of Chromosomal Imbalance and Phenotype in Humans Using Ensembl Resources. American journal of human genetics 84, 524-533.
93. Eijkenboom, D.F., Verbist, B.M., Cremers, C.W., and Kunst, H.P. (2012). Bilateral conductive hearing impairment with hyperostosis of the temporal bone: a new finding in Robinow syndrome. Archives of otolaryngology--head & neck surgery 138, 309-312.
94. Beiraghi, S., Leon-Salazar, V., Larson, B.E., John, M.T., Cunningham, M.L., Petryk, A., and Lohr, J.L. (2011). Craniofacial and intraoral phenotype of Robinow syndrome forms. Clinical genetics 80, 15-24.

95. Willert, K., Brown, J.D., Danenberg, E., Duncan, A.W., Weissman, I.L., Reya, T., Yates, J.R., 3rd, and Nusse, R. (2003). Wnt proteins are lipid-modified and can act as stem cell growth factors. Nature 423, 448-452.
96. Adzhubei, I.A., Schmidt, S., Peshkin, L., Ramensky, V.E., Gerasimova, A., Bork, P., Kondrashov, A.S., and Sunyaev, S.R. (2010). A method and server for predicting damaging missense mutations. Nature methods 7, 248-249.
97. Wilkins, M.R., Gasteiger, E., Bairoch, A., Sanchez, J.C., Williams, K.L., Appel, R.D., and Hochstrasser, D.F. (1999). Protein identification and analysis tools in the ExPASy server. Methods in molecular biology 112, 531-552.
98. Kozlowski, L.P. (2007-2013). Isoelectric Point Calculator. In. (
99. Korinek, V., Barker, N., Willert, K., Molenaar, M., Roose, J., Wagenaar, G., Markman, M., Lamers, W., Destree, O., and Clevers, H. (1998). Two members of the Tcf family implicated in Wnt/beta-catenin signaling during embryogenesis in the mouse. Molecular and cellular biology 18, 1248-1256.
100. Polder, B.J., Van't Hof, M.A., Van der Linden, F.P., and Kuijpers-Jagtman, A.M. (2004). A meta-analysis of the prevalence of dental agenesis of permanent teeth. Community dentistry and oral epidemiology 32, 217-226.
101. De Coster, P.J., Marks, L.A., Martens, L.C., and Huysseune, A. (2009). Dental agenesis: genetic and clinical perspectives. Journal of oral pathology & medicine : official publication of the International Association of Oral Pathologists and the American Academy of Oral Pathology 38, 1-17.
102. Khajavi, M., Inoue, K., and Lupski, J.R. (2006). Nonsense-mediated mRNA decay modulates clinical outcome of genetic disease. European journal of human genetics : EJHG 14, 1074-1081.
103. Gonzalez-Sancho, J.M., Brennan, K.R., Castelo-Soccio, L.A., and Brown, A.M. (2004). Wnt proteins induce dishevelled phosphorylation via an LRP5/6-independent mechanism, irrespective of their ability to stabilize beta-catenin. Molecular and cellular biology 24, 4757-4768.
104. Zhu, S., Liu, L., Korzh, V., Gong, Z., and Low, B.C. (2006). RhoA acts downstream of Wnt5 and Wnt11 to regulate convergence and extension movements by involving effectors Rho kinase and Diaphanous: use of zebrafish as an in vivo model for GTPase signaling. Cellular signalling 18, 359-372.
105. Tree, D.R., Shulman, J.M., Rousset, R., Scott, M.P., Gubb, D., and Axelrod, J.D. (2002). Prickle mediates feedback amplification to generate asymmetric planar cell polarity signaling. Cell 109, 371-381.

9. APPENDIX

RT-PCR of DVL1 from Case 1 (summer studentship work)

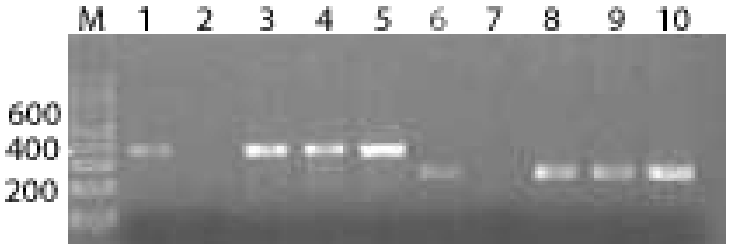

Fig1, lanes 1-5 are with the APRT primers, and lanes 6-10 are with the CREB primers. 1. positive control using cDNA previously synthesised in the lab, 2. negative control, 3. patient cDNA, 4. control one cDNA, 5. control two cDNA, 6-10 are repeats of the above.